

Review article

## A review on modeling strategies in understanding the process mechanism of 3D printed continuous fiber-reinforced thermoplastic composites

Shenru Wang<sup>a</sup>, Xin Yan<sup>a,b,\*</sup>, Baoning Chang<sup>b,e</sup>, Jiae Zhang<sup>f</sup>, Siqin Liu<sup>a</sup>, Fei Liu<sup>a</sup>, Junfan Shang<sup>a</sup>, Li-Hua Shao<sup>c</sup>, Sha Yin<sup>c</sup>, Wuxiang Zhang<sup>a,b,\*</sup>, Yingdan Zhu<sup>d,\*</sup>, Xilun Ding<sup>a,b</sup>

<sup>a</sup> School of Mechanical Engineering and Automation, Beihang University, Beijing, 100191, China

<sup>b</sup> Ningbo Institute of Technology, Beihang University, Ningbo, 315832, China

<sup>c</sup> School of Aeronautic Science and Engineering, Beihang University, Beijing, 100191, China

<sup>d</sup> Ningbo Institute of Material Technology and Engineering, Chinese Academy of Sciences, Ningbo, 315201, China

<sup>e</sup> State Key Laboratory of Structural Analysis, Optimization, and CAE software for Industrial Equipment, Dalian University of Technology, Dalian, 116023, China

<sup>f</sup> Key Laboratory of Aviation Science and Technology for Digital Manufacturing Techniques, AVIC Manufacturing Technology Institute, Beijing, 100024, China



### ARTICLE INFO

**Keywords:**

Continuous fiber  
3D printing  
Process modeling  
Multiscale modeling  
Mechanical properties

### ABSTRACT

Continuous fiber 3D printing (CF3DP) has emerged as a promising technique that deposits continuous fiber alongside resin, offering numerous functional and intelligent applications. CF3DP involves rapid heating and cooling of materials, characterized by multiscale and multiphase nature, which complicates the understanding of the underlying process mechanisms. This difficulty hinders the prediction and control of the manufacturing defects and may lead to the compromise of mechanical properties. Although significant efforts have been made in process modeling to establish the relationship between process parameters and manufacturing performance, a systematic review of these studies remains absent. In this work, we attempted to provide an overview of the modeling strategies in understanding the process mechanism of CF3DP. The various physical phenomena involved in the CF3DP process are systematically analyzed and the corresponding modeling studies are summarized. Then, special attention is devoted to exploring how multiscale modeling approaches can establish a relational framework between the CF3DP process and the prediction of mechanical properties. This article also discusses the modeling strategies of failure behaviors considering the manufacturing defects. Finally, this paper discusses emerging applications of CF3DP and highlights the critical role of process modeling in driving future advancements. With the discussion of the process modeling strategies in CF3DP, researchers can identify appropriate methods tailored to their specific interests while gaining deeper insights into the underlying process mechanism.

### 1. Introduction

Continuous fiber-reinforced thermoplastic composites (CFRTPCs) are attractive for various applications, ranging from aerospace to ground transportation, due to their distinct advantages of high fracture toughness, high impact resistance, and recyclability [1–4]. Due to these superior advantages, the rapid automated manufacturing of CFRTPC components has attracted considerable interest in various industries. Automated manufacturing processes such as filament winding [5] and automated fiber placement [6] have been widely adopted in different sectors. However, due to the inherent process limitations, these conventional manufacturing processes face challenges in the automated manufacturing of load-bearing structural parts with small dimensions and complex geometries [7]. Consequently, to fill the market gaps in composites with intricate structures and functional

requirements, the continuous fiber 3D printing (CF3DP) technique has emerged as a promising technique, with advantages such as high production efficiency, minimal material waste, and the capacity to fabricate components with complex geometries [8–20].

CF3DP builds upon the fused deposition modeling (FDM), which relies on the rapid heating of CFRTPCs above their melting temperature, followed by fusing the adjacent material surfaces during the subsequent layer-by-layer deposition process [21,22], as shown in Fig. 1. This schematic diagram provides two typical approaches used in CF3DP: towpreg pultrusion (Fig. 1a) and in-situ impregnation (Fig. 1b). In both approaches, raw materials are transported to the molten cavity and then heated to the molten state [9,22]. With movement of the print head, the thermoplastic resin envelops the continuous fiber, and both are pulled out of the nozzle. Once the material leaves the

\* Corresponding authors.

E-mail addresses: [yan\\_xin@buaa.edu.cn](mailto:yan_xin@buaa.edu.cn) (X. Yan), [zhangwuxiang@buaa.edu.cn](mailto:zhangwuxiang@buaa.edu.cn) (W. Zhang), [y.zhu@nimte.ac.cn](mailto:y.zhu@nimte.ac.cn) (Y. Zhu).

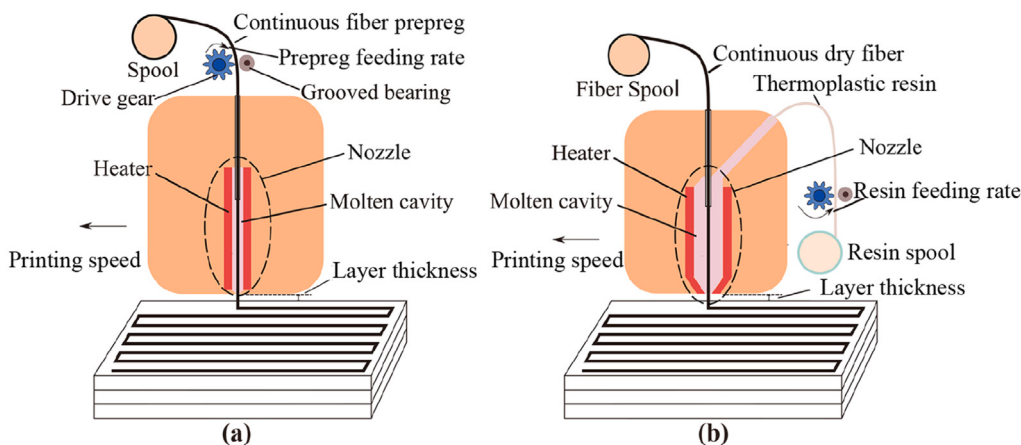


**Fig. 1.** Illustration for two types of approaches used for CFRTPC printing: (a) towpreg pultrusion approach; (b) in-situ impregnation approach.

print head, it cools and solidifies to form a structure. The significant difference between these two approaches lies in the raw materials used in manufacturing. The towpreg pultrusion approach utilizes the prepreg [23,24], while the in-situ impregnation approach utilizes the dry fiber (unimpregnated fiber) and thermoplastic resin, with impregnation occurring within the print head [25–28]. Particularly, the in-situ impregnation approach enables the printing of composites with various fiber volume percentages by controlling the printing speed and resin feeding rate [28].

The manufacturing performance of the CF3DP is heavily influenced by its manufacturing process [15,29,30]. This process governs the flow, bonding, solidification, and crystallization of materials during printing, all of which are closely linked to the internal defects and material properties of the final printed structures [16,23,29,31–36]. Currently, one of the primary obstacles that hinders the broad application of CF3DP in industry is the unstable processing quality, which arises from the lack of clarity in the underlying process mechanisms [37–40]. Numerous experimental studies have shown that optimizing process parameters such as printing temperature [25,29,36,40], printing speed [36,41], and layer thickness [25,29,42,43] can reduce defects and significantly improve manufacturing performance. The aforementioned studies adopted manufacturing trials on representative structural components to optimize process parameters [44]. However, given the multitude of commercially available thermoplastic composite materials, along with specific structural designs and equipment facilities, it becomes impractical to conduct trials for every combination of processing conditions. It is also challenging to understand the process mechanism comprehensively and to determine suitable values for the process parameters solely through experiments [38,39]. These challenges arise because of difficulties in accurately measuring the micro properties of the CF3DP process encompassing multiscale and multifield characteristics [38]. Therefore, process modeling of CF3DP is essential for understanding the process mechanism and capturing the relationship between the processing conditions and manufacturing performance.

Process modeling entails analyzing the physical phenomena inherent in the CF3DP process and predicting the mechanical properties as well as the failure behaviors of the printed parts [13,38,39,44–47]. It has the unique capability to capture the dynamic evolution of the CF3DP process, which presents considerable challenges for experimental observations [38,45,47]. In recent years, many studies concentrating on process modeling have been performed to explore the underlying process mechanism from different aspects, such as melt flow [38], fluid–structure interaction [48], impregnation [39,49], and warpage [36]. Given the complexity of the physical phenomena involved and the diverse modeling techniques adopted, there is an urgent need for a systematic review to help researchers identify the critical

factors and suitable methods relevant to their specific interests, thereby facilitating subsequent process modeling research.

This paper offers a comprehensive review of the process modeling methodologies applied to the CF3DP process. Section 2 discusses how the dominant process parameters affect the printing performance by influencing the physical phenomena. Section 3 provides a comprehensive summary and discussion of the physical phenomena inherent in CF3DP, along with process modeling that establishes the relationship between the process parameters and the physical phenomena. Section 4 highlights recent advances in the multiscale modeling within the process modeling, providing an intuitive understanding of how processing conditions affect the printing performance. Section 5 discusses the failure modes and mechanisms caused by different manufacturing defects, coupled with modeling approaches. Finally, the emerging applications and challenges of CF3DP are presented and discussed.

## 2. Dominant process parameters

Process parameters refer to controllable factors that directly affect the CF3DP process, and subsequently the precision and properties of the printed parts [9,25,26]. Through extensive experimental research, researchers have gained initial insight into the effects of process parameters on part performance [9,22,25]. The observed performance variations related to the process parameters in these experiments have prompted the exploration of forming mechanism through process modeling. In this section, we summarize several key process parameters that influence the CF3DP process and discuss their effects on the properties of the printed parts.

### 2.1. Printing speed

The printing speed refers to the velocity at which the print head moves (as shown in Fig. 1) [9]. It has a significant effect on the printing accuracy, part quality, and manufacturing efficiency. High printing speeds lead to insufficient solidification time, which can cause fiber displacement within the molten resin, especially at the corners of the path [50], as shown in Fig. 2a. This displacement may cause the fiber to deviate from the predefined fiber path, thereby reducing the printing precision. At elevated printing speeds, the time available for inter-filament bonding is curtailed, leading to compromised adhesion and increased porosity [51]. A faster printing speed also shortens the duration of fiber/matrix impregnation, diminishing the interaction between fiber and resin, which is critical to the mechanical properties of composites [27,52]. Consequently, printing at low speeds is generally associated with enhanced mechanical properties. However, it is crucial to acknowledge that an exceedingly slow printing speed substantially increases the production time, which is a drawback for

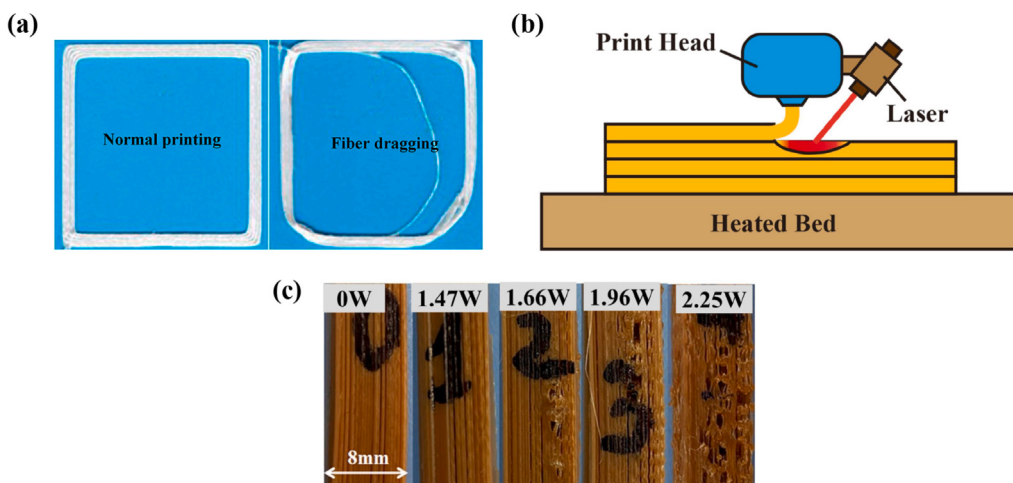


**Fig. 2.** (a) Schematic diagram of fiber dragging (adapted from [50]); (b) heating sources of CF3DP; (c) images of specimens with different laser power (reproduced from [64]). Adapted/reproduced with permission.

efficiency [9]. Therefore, it is necessary to balance the relationship between the printing quality and efficiency to determine the appropriate printing speed. Based on a summary of previous studies, an appropriate range for the printing speed to achieve better product performance is 60–240 mm/min [14,25–27,50,53–61].

Specifically, for the in-situ impregnation approach, the feeding rate (Fig. 1b) — which represents the velocity at which the resin filament is delivered to the nozzle — is another crucial factor that demands careful consideration in determining the appropriate printing speed value. The feeding rate directly determines the inner pressure within the nozzle [25]. A high feeding rate delivers a large amount of resin to the nozzle, leading to increased inner pressure, which in turn minimizes the appearance of bubbles within the composite [25,27,51,62,63]. However, in a practical printing process, the feeding rate cannot be blindly increased. Geng et al. [63] observed that excessive inner pressure caused the melt to flow upward along the throat pipe, obstructing the channel of resin feeding.

In engineering applications, the printing speed and the feeding rate should be synchronized to avoid poor performance of printed parts [25,26,51,63]. In the towpreg pultrusion approach, the feeding rate should be equal to the printing speed [51]. In the in-situ impregnation approach, the relationship between the feeding rate and printing speed is determined by considering equal material volumes for both feeding and extrusion within the nozzle [58]:

$$F_E \propto F_D (H L - S_f) / (\pi R_m^2) \quad (1)$$

where,  $F_E$  is the feeding rate of resin filament;  $F_D$  is the printing speed;  $H$  is the hatch spacing;  $L$  is the layer thickness;  $S_f$  is the cross-sectional area of the fiber bundle; and  $R_m$  is the radius of the resin filament. This formula establishes an approximate correlation between the printing speed and feeding rate, providing valuable insight when working with new materials or new structural designs. Using this formula, one can calculate a reference speed and then fine-tune the speed based on the printing results.

## 2.2. Forming temperature

The forming temperature refers to the temperature required during the CF3DP process. The printing process of CFRTPCs involves the heating and cooling of the resin, and the forming temperature significantly affects the printing quality [25,53,54]. The forming temperature is primarily composed of the printing temperature, the heated bed temperature, and the auxiliary heat temperature, as shown in Fig. 2b.

As the material enters the print head, it undergoes heating by a heater (typically a resistive heating block) and transforms into a

molten state (Fig. 1). The heater is the primary heat source during the CF3DP process; thus, its temperature is termed the printing temperature [25,53,54]. According to diffusion theory, high printing temperature improves the thermal motion of polymer chains, promoting adhesion between the printed filaments [65]. High printing temperature also facilitates improved fiber/matrix impregnation due to the increased fluidity of the molten resin, which leads to a well-bonded interface [22,66]. However, an overly elevated printing temperature can result in excessive fluidity of the molten resin, causing it to flow out from the nozzle due to gravity, thereby compromising the printing precision [25,66]. The thermal decomposition of the resin also occurs at an excessively elevated temperature [66]. Hence, the optimal printing temperature should allow the molten resin to flow and bond effectively without causing excessive liquefaction [51]. The specific printing temperature varies depending on the resin adopted. In summary, the appropriate printing temperatures for common thermoplastic resins are listed in Table 1 based on previous research.

When the molten material leaves the print head, it is deposited on the heated bed and undergoes rapid cooling and solidification, which results in accumulation of residual stress [101]. The residual stress can cause warpage deformation in the structure, which seriously affects the dimensional precision of the printed parts [35,36,101]. It is common to utilize a heated bed (Fig. 2b) to reduce the temperature gradient during the cooling process, thereby mitigating the warpage deformation [35,36,102,103]. The heated bed temperature should be slightly above the glass transition temperature of the resin [102]. A significantly higher heated bed temperature may lead to excessive softening of the printing material, thus seriously affecting the continuous printing [104]. Table 1 summarizes the recommended heated bed temperatures.

Moreover, an auxiliary heat source, often a laser (Fig. 2b), is commonly utilized to enhance the interlayer bonding strength [80,105–107]. By preheating the area along the filament deposition path with a laser, the localized surface temperature (laser point temperature) rises above the resin's glass transition temperature. This elevation in temperature increases the flexibility of the molecular chain, thereby improving the interlayer adhesion [80]. The quality of the printed part is quite sensitive to the laser point temperature, since the excessive heat may lead to resin evaporation, which forms the void defect (Fig. 2c) [64,69,80]. The laser point temperature is primarily determined by the printing speed and laser power [108]. Based on previous research, reducing the printing speed or increasing the laser power would bring the laser point temperature above the resin's decomposition temperature, which would yield the resin evaporation [109]. Researchers utilized the infrared thermal imager to identify the optimal laser point temperature [69,80]. Besides, theoretical model [108] and numerical

**Table 1**  
Recommended forming temperatures for different thermoplastic resins (unit is °C).

| Materials                         | Melting points | Glass transition temperatures | Printing temperatures | Heated bed temperatures | Laser point temperatures |
|-----------------------------------|----------------|-------------------------------|-----------------------|-------------------------|--------------------------|
| PLA <sup>a</sup> [25,55,56,67–69] | 174            | 62                            | 200–230               | 60–80                   | 145                      |
| ABS <sup>b</sup> [27,70–73]       | –              | 105                           | 230–250               | 90–110                  | –                        |
| PA <sup>c</sup> [57,74–79]        | 220            | 48                            | 260–290               | 50–80                   | –                        |
| PEEK <sup>d</sup> [61,63,80–82]   | 343            | 143                           | 360–420               | 136–150                 | 400                      |
| PC <sup>e</sup> [83–86]           | –              | 121                           | 255–270               | 80–120                  | –                        |
| PET <sup>f</sup> [87,88]          | 240            | 80                            | 250–260               | 65–85                   | –                        |
| PETG <sup>g</sup> [30,89–92]      | –              | 77                            | 230–250               | 65–90                   | –                        |
| ASA <sup>h</sup> [93–96]          | –              | 103                           | 240–260               | 90–110                  | –                        |
| PP <sup>i</sup> [97–100]          | 165            | –15                           | 220–250               | 60–80                   | –                        |

<sup>a</sup> Polylactic acid.

<sup>b</sup> Acrylonitrile butadiene styrene.

<sup>c</sup> Polyamide.

<sup>d</sup> Polyether ether ketone.

<sup>e</sup> Polycarbonate.

<sup>f</sup> Polyethylene terephthalate.

<sup>g</sup> Polyethylene terephthalate glycol.

<sup>h</sup> Acrylonitrile styrene acrylate.

<sup>i</sup> Polypropylene.

simulation [39,109–111] were reported to study the effects of printing speed and laser power on the laser point temperature. Table 1 summarizes the recommended laser point temperatures.

### 2.3. Forming pressure

The forming pressure refers to the force exerted on the printed material during the layer-by-layer printing process [39], which is closely associated with the interlayer bonding strength [34,39]. In the context of CF3DP, the forming pressure is primarily regulated by the layer thickness [52,112]. The layer thickness is defined as the vertical distance between the nozzle and the printing surface (Fig. 1) [25]. As reported in previous research, the forming pressure decreases with the increased layer thickness [43], which results in enhanced porosity and reduced interfacial bonding in the printed parts [22,25,113]. Hence, the layer thickness should be sufficiently thin to ensure the forming pressure needed for high-quality printing. However, if the layer thickness is excessively small, the molten resin may overflow and re-enter the feeding tube, leading to a blockage [52]. The overly thin layer also exerts an excessive compaction force on the printed filament, resulting in the fiber scratch and breakage [114]. Based on the summary of previous studies, the recommended range of layer thickness falls between 0.15 mm and 0.4 mm [14,26,27,53,53–58,115,116].

Sometimes, the forming pressure provided by adjusting the layer thickness is below the requirement to form a reasonable interfacial bond, which results in high porosity and weak interface in the printed parts [16,23,33,34]. To increase the forming pressure, some researchers introduced a roller to the printer, which could notably decrease the porosity of printed parts to approximately 3% [33]. However, it is important to note that the involvement of roller, which is quite similar to the automated fiber placement,<sup>1</sup> increases the complexity of the equipment and reduces the flexibility of the system in manufacturing intricate structural components.

<sup>1</sup> We remark that with the involvement of roller, it actually makes the CF3DP into automated fiber placement, except using different heating strategies. For automated fiber placement, the dominant heating strategy is laser or other radiative heat approaches, whereas for CF3DP, the resin is usually heated with a resistive heater located near the nozzle.

### 2.4. Discussion

To facilitate rapid reference and understanding of the information, we have compiled a summary of how the aforementioned process parameters affect printing performance. Additionally, we list suggested parameter values for common thermoplastics. For detailed information, please refer to Table 2. However, it is important to note that these parameter values are provided solely as a reference. Readers should adjust them according to their particular printing circumstances.

Section 2 provides a qualitative overview of the relationships between various process parameters and printing performance, highlighting the key factors that should be considered when designing appropriate values for these process parameters. These factors reflect the physical phenomena associated with the CF3DP process. The overarching goal is to establish a clear link between process parameters and printing performance, a challenge that researchers have been striving to address for years. In the following sections, we will explore how physical phenomena can serve as a bridge between process parameters and printing performance. By constructing a framework that connects the process parameters, physical phenomena, and printing performance, we aim to identify the optimal process parameters needed to achieve the desired printing outcomes based on a solid understanding of the underlying printing mechanisms.

### 3. Process modeling of continuous fiber 3D printing

As described in the introduction, the CF3DP process is a variant of the FDM technology, and the integration of continuous fiber adds additional complexity. The entire CF3DP process involves various phase transitions and physical interactions. Specifically, the CF3DP process can be divided into two stages: the intra-nozzle process and the deposition process, as illustrated in Fig. 3. We would like to highlight that the process mechanisms of the two types of CF3DP exhibit slight differences. These distinctions will be addressed in detail during the discussion of the two stages of the CF3DP process.

During the intra-nozzle stage, the material is delivered to a high-temperature nozzle by the drive gear, where it melts and transitions from a solid to a liquid state. In the towpreg pultrusion approach (Fig. 1a), the drive gear feeds the prepreg filament into the nozzle at a rate equal to the printing speed. The impregnated resin within the prepreg melts upon entering the nozzle and is pulled out along with the fiber, without forming a resin flow field inside the nozzle [117]. Whereas, for the in-situ impregnation approach (Fig. 1b), the drive gear feeds

**Table 2**  
Effect summary of the process parameters.

| Process parameters                          | Effects at low value  | Effects at high value   | Recommended values                                      |
|---|---|---|---|
| Printing speed [9,27,50–52]                 | Well-bonded interface; Low porosity; Low efficiency                                 | Insufficient solidification time; Poor interface  | 60–240 mm/min   |
| Feeding rate [25–27,58,62, 63]              | Increased bubbles   | Increased nozzle's inner pressure; Reduced bubbles<br><b>Excessive high value:</b><br>Resin backflow and feed channel obstruction | synchronized with printing speed (refer to Section 2.1) |
| Printing temperature [22,25,65,66]          | Poor interface  | Well-bonded interface; Elevated impregnation<br><b>Excessive high value:</b><br>Resin thermal decomposition                       | (refer to Table 1)                                      |
| Heated bed temperature [35,36,102,103]      | Warpage   | Mitigated warpage<br><b>Excessive high value:</b><br>Excessive softening of part  | (refer to Table 1)                                      |
| Laser point temperature [39, 64,80,108,109] | Poor interface  | Well-bonded interface<br><b>Excessive high value:</b><br>Resin evaporation  | (refer to Table 1)                                      |
| Layer thickness [22,25,43,52, 113,114]      | Well-bonded interface; Low porosity<br><b>Excessive low value:</b><br>Fiber scratch | Enhanced porosity; Poor interface   | 0.15–0.4 mm   |

the thermoplastic resin filament into the nozzle at a rate determined by the printing speed and the resin extrusion volume [58] (as described in Eq. (1)). The molten resin forms a flow field inside the nozzle and envelops the dry fiber bundle [25]. Subsequently, both the fiber bundle and its coated resin are pulled out of the nozzle. Therefore, the intra-nozzle process of the in-situ impregnation approach is more complex, and research on process modeling primarily focuses on this approach. A detailed discussion of the process mechanisms and modeling methods involved in the intra-nozzle stage is provided in Section 3.1.

During the deposition stage, the fiber and resin are pulled from the nozzle and deposited onto the heated bed. Particularly, for the in-situ impregnation approach, the resin can be additionally extruded by the drive gear, which enables the printing of complex curved structures [118]. Following deposition, the resin rapidly cools and solidifies through heat exchange with the surrounding environment and contact surfaces. A detailed discussion of the process mechanisms and modeling methods involved in the deposition stage is provided in Section 3.2.

Overall, the deposition process phenomena of towpreg pultrusion and in-situ impregnation share some similarity, allowing related process modeling studies to be applicable to both. However, since the in-situ impregnation approach involves the resin flow field within the nozzle and the fiber/matrix impregnation happening during the deposition process, the intra-nozzle modeling and fiber/matrix impregnation modeling are primarily relevant to the in-situ impregnation approach, which will be discussed in Sections 3.1 and 3.2.4, respectively.

### 3.1. Intra-nozzle process

In the intra-nozzle process, the thermoplastic resin is heated to a molten state and flows under the propulsion of the feeding resin. Meanwhile, the continuous fiber within the molten resin deforms under the viscous forces exerted by the surrounding resin, while this deformation, in turn, influences the flow of the resin [119]. Hence, the intra-nozzle process is a fluid–structure interaction (FSI) problem [48], which encompasses three dominant physical phenomena: melt flow, fiber deformation, and FSI (as illustrated in Fig. 3). In this section, we will delve into the relevant modeling studies concerning the intra-nozzle process from the aforementioned three perspectives. The melt flow part focuses on elucidating the flow behavior of the molten resin. The fiber deformation part focuses on the structural behavior of the flexible fiber, and the FSI part delves into the interaction between the fiber and the molten resin.

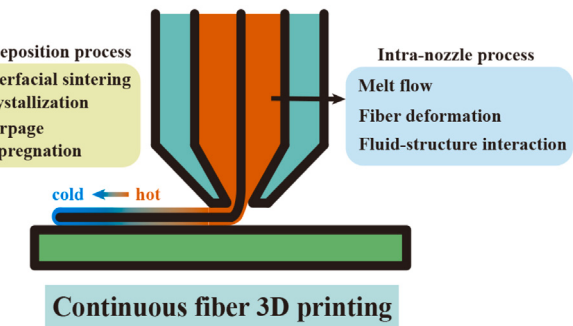


Fig. 3. Physical phenomena involved in the continuous fiber 3D printing process.

#### 3.1.1. Melt flow

The schematic diagram of the hot end assembly is illustrated in Fig. 4a. The nozzle maintains a high temperature throughout the printing process. When the resin enters the liquefier zone within the nozzle, it is gradually heated to a molten state and then flows through the nozzle, propelled by the feeding resin. Driven by the feeding resin, the molten resin flows into the funnel-shaped conical transition zone, where it is constricted to a suitable printing diameter and extruded from the capillary.

Notably, in this scenario, the contribution of fiber is not taken into account. Considering the similarities between this simplified scenario and FDM, the approaches employed in FDM can be adapted and applied in this context [120–124]. Based on the fundamental fluid governing equations, the analytical model by Bellini [125] was developed to calculate the force required to push the filament through the nozzle. As shown in Fig. 4b, the Bellini's model assumes that once the thermoplastic resin enters the nozzle, it transitions into a molten state. Hence, the Bellini's model is primarily suited for lower filament feeding rates, below 0.25 mm/s, which allows sufficient time for resin melting [126]. However, in practical applications, higher filament feeding rates (above 1 mm/s) are commonly employed to increase efficiency [127]. In this situation, Osswald's model [126] was developed, which assumes the melt region is compressed into a melt film within the conical transition region due to the insufficient heating time, as illustrated in Fig. 4b.

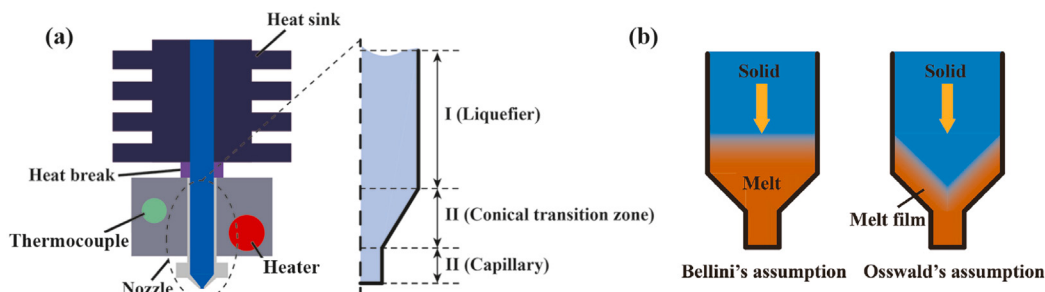


Fig. 4. (a) Schematic diagram of the hot end assembly; (b) schematic diagrams of Bellini's assumption and Osswald's assumption.

These analytical models focus on the evaluation of pressure drop and flow rate [128] without providing a complete scenario of the fluid field. This can be resolved using advanced numerical approaches, such as the finite volume method (FVM) [38,129,130] and smoothed particle hydrodynamics (SPH) [48]. These numerical approaches start with a geometric model based on the nozzle structure and adopt the appropriate flow mode according to the actual printing situation. Typically, the flow mode during FDM is laminar [38,128,131]. After that, process parameters, such as forming temperature and printing speed, are inputted into the numerical system as boundary conditions. Before the fluid equations are numerically solved through the aforementioned approaches, the rheological behavior of the resin should be carefully considered. The resin commonly used in the CF3DP process exhibits shear-thinning behavior, and its viscosity is primarily influenced by temperature and shear rate [132]. For the temperature effect, the Arrhenius [131] and Williams-Landel-Ferry [38,120,121] models are frequently employed to characterize the temperature dependence of viscosity. The shear rate dependent behavior of viscosity is typically described using the generalized newtonian fluid models, such as power-law [120,131], Cross [121], and Carreau [122,123,123]. Moreover, considering the viscoelastic effect of molten resin, some studies introduced viscoelastic models to more accurately characterize the flow behavior of the molten resin [120,123,133]. In addition, for CFRTPCs, the presence of continuous fiber also influences the viscosity of the molten resin [134]. Due to the high anisotropy of the continuous fiber, the composite exhibits diverse viscosity along the longitudinal and transverse directions [134]. The viscosity is also influenced by the fiber volume fraction and the fiber arrangement [134]. For more detailed information, please refer to these reviews [134,135].

### 3.1.2. Fiber deformation

Besides the flow of the molten resin, the structural behavior of the continuous fiber within the molten resin is also an important factor. The fiber undergoes deformation due to the viscous forces exerted by the surrounding resin [119]. Unlike the modeling of chopped fibers, which usually relies on the assumptions of rigid body behavior [136] or orientation homogenization [137,138], modeling of continuous fiber meets the challenges of considering the anisotropic nature and flexibility [48]. To accurately describe the structural behavior of the continuous fiber, several modeling approaches have been employed, which can be divided into two categories: mesh-based approaches (such as the finite element method (FEM) [129,139]) and mesh-free approaches (such as the discrete element method (DEM) [48]). The mesh-based approaches operate under the continuous medium hypothesis [140] and partition the computational domain into meshes. These approaches calculate fiber deformation and stress by tracking the motion of mesh nodes. Despite their computational efficiency, the mesh-based approaches struggle to capture the flexible movement (bending and twisting) of continuous fiber due to the mesh distortion [48,141]. Conversely, the mesh-free approaches can solve this problem by representing continuous fiber using discrete particles, which notably increases the freedom of the fiber model [48]. However, this increased freedom also leads to excessive computational costs.

### 3.1.3. Fluid–structure interaction

Based on the modeling strategies of the molten resin and the deformed fiber, the FSI problem can be divided into three cases.

When the flow behavior of the molten resin is characterized by mesh-based approaches (typically FVM) [38,129,130] and the structural behavior of the continuous fiber is represented by mesh-based approaches (typically FEM) [129,139], the challenge in this case is the information transfer on the boundary between the fluid and structural domains. There are two common methods for handling this problem: the Arbitrary Lagrangian–Eulerian (ALE) and the Immersed Boundary Method (IBM) [142–144]. The ALE employs a unified mesh in both the fluid and structural domains, which can accurately exchange information through the shared mesh on the boundary [141,145]. However, because of the constraints imposed by the Eulerian mesh of the fluid, the Lagrangian mesh of the structure cannot experience large deformation. Hence, this method fails to capture the large deformation of the fiber [143,145]. To address this issue, the IBM offers an alternative by adopting separate meshes for the fluid and the structural domains. This enables information exchange by interpolating the interaction force into the governing equations of fluid and structural models within the boundary region [146].

For the structural model considering the flexible movement, the continuous fiber can be represented as a series of discrete particles, utilizing mesh-free approaches like DEM. In this case, it is imperative to describe the interaction between the flow behavior of the resin characterized by FVM and the structural behavior of the particle-based fiber [147]. The influence of the molten resin on the continuous fiber can be considered by interpolating the interaction force into the governing equation of the DEM at the boundary. However, it is challenging to apply the influence of fiber on the molten resin, because the fiber force is non-continuous for the continuous entity of the fluid model [147].

To account for the influence of fiber deformation on the molten resin, the DEM-SPH coupling approach serves as a viable alternative [48]. In this case, the flow behavior of the molten resin is characterized by mesh-free approaches like SPH, while the structural behavior of the continuous fiber is represented by DEM. Both the fluid and structural domains are described by discrete particles, facilitating convenient information exchange through the application of interaction forces to the corresponding particles of the molten resin and the continuous fiber. For example, as depicted in Fig. 5, Yang et al. [48] utilized this DEM-SPH coupling approach to simulate the bending deformation and stress of the continuous fiber during the intra-nozzle process, thus aiding in the structural optimization of the nozzle.

### 3.2. Deposition process

When the printing material is pulled from the nozzle, it undergoes the deposition process and forms the composite structure. This process is crucial in determining the printing quality and has attracted tremendous attention. In the deposition process, the molten resin is deposited onto the heated bed and undergoes a rapid temperature reduction with flow. Hence, it is a coupled process influenced by multiple fields, such

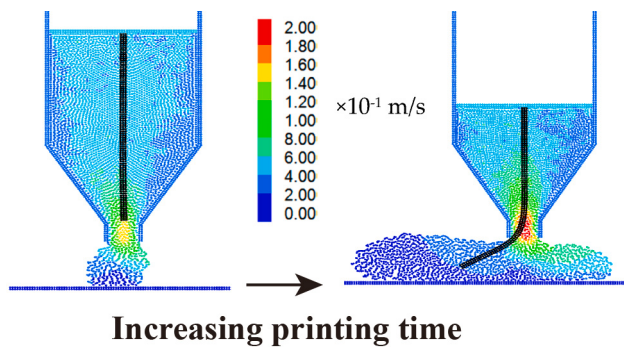


**Fig. 5.** The simulation of fiber movement and resin flow during the intra-nozzle process in CF3DP (with the cloud chart depicting the resin flow velocity) [48]. Reproduced with permission.

as thermal [36,66], fluid [38,48], and stress [49]. In order to understand this complicated process as well as its underlying mechanism, the deposition process can be analyzed from two perspectives: the thermal process (rapid cooling) and the fluid flow process (flow of the molten resin).

During the rapid cooling process, the temperature of the deposited material rapidly decreases from the printing temperature to the ambient temperature [148,149]. As a result, the molten resin solidifies quickly to form the structure. Various forms of heat transfer are involved in this process, including convection with the surrounding environment, conduction with the heated bed, and conduction between adjacent filaments [113,150,151], as illustrated in Fig. 6a. A series of studies have been carried out to capture the temperature evolution, utilizing both analytical [150,151] and numerical models [36, 39,152–155]. Particularly, because the presence of fiber introduces anisotropy in thermal properties, some researchers have employed effective medium approximation [156–159] and micromechanics [159–161] approaches to estimate the thermal properties of composite materials. Effective medium approximation approaches model composites as homogeneous media by employing weighted averaging technique based on material properties, fiber volume fractions, and fiber geometrical characteristics [156,162]. When fibers are uniformly distributed within the resin phase, the composite can be treated as a homogeneous medium [156,163]. In this situation, the effective medium approximation approaches provide a rapid and effective estimation of the thermal properties. However, their effectiveness is limited when applied to composites with heterogeneous fiber distributions [159,160, 164]. To address this limitation, micromechanics approaches describe the composite heterogeneity by resolving local thermal interactions at the microstructural level [160,161]. In this way, the micromechanics approaches allow for the incorporation of microstructural characteristics into the prediction of thermal properties, resulting in greater accuracy. However, this comes at the cost of significantly increased computational complexity.

During the fluid flow process, the semi-molten resin flows under the force exerted by the print head, as presented in Fig. 6b. The resin flow promotes the bonding between the deposited filaments by filling the spaces between them [38]. Numerous studies have been performed to reproduce this process, investigating the effect of printing parameters on the shape and porosity of the deposited material using numerical methods [38,165,167,168]. Particularly, surface-tracking techniques like volume-of-fluid [165,168,169] have been utilized to capture the fluid surface, enabling dynamic visualization of the fluid flow. Furthermore, the viscoelastic effect of the resin is another important factor to consider in deposition simulations. This effect decreases the flowability of the resin and leads to swelling [166], as depicted in Fig. 6c.

Incorporating the various models of thermal and fluid flow, researchers have obtained several valuable insights into how the printing

parameters (layer thickness, printing temperature, and printing speed) affect the quality of the deposited materials and overall structure [38, 165,167,168,170,171]. Specifically, the layer thickness determines the magnitude of the external forces driving the material flow [165]; the printing temperature affects the viscosity of the molten material [38]; and the printing speed is correlated with the material flow time [38, 165]. A low layer thickness and the corresponding high pressure promote the material flow (shown in Fig. 6b) [165], thus facilitating the void filling and increased interfacial bonding [38]. The increased viscosity as a result of a low temperature can impede the material flow. A slow printing speed allows more time for the material to flow under pressure, which helps reduce the porosity [38,165].

Furthermore, during the deposition process, there are multiple physical phenomena that are crucial in determining the printing quality, including interfacial sintering [113,148,172], crystallization [149,173, 174], warpage [36], and impregnation [39,49]. These physical phenomena are closely related to the temperature distribution and flow morphology during the CF3DP process, which can be obtained from the thermal and flow analyses mentioned above.

### 3.2.1. Interfacial sintering

Interfacial sintering is a phenomenon involving the coalescence of particles [113,148], which is driven by the heat energy of the molten material [113,172]. When the molten material is pulled out of the nozzle and deposited onto the previously deposited material, heat is transferred from the hot area to the cold area [149]. This heat transfer partially melts the solidified structure adjacent to the newly deposited material, thus causing the interfacial bonding (Fig. 7a) [149,172]. Hence, interfacial sintering plays a crucial role in determining the interfacial bonding strength and porosity of the printed parts [66].

Typically, the analysis of interfacial sintering has been performed utilizing the Frenkel model and its modified models, which have been derived by assuming that the work of surface tension is equal to the work of viscous dissipation, while other external forces, such as gravity, are neglected [66,113,175]. For the CF3DP process, the addition of continuous fiber alters the physical parameters during heat transfer, influencing the size of the bonding neck between the printed filaments (Fig. 7a) [66]. With this in mind, Fan et al. [66] proposed an analytical model to investigate the forming mechanism of the interfacial bonding neck during the CF3DP process. Their findings revealed that an elevated printing temperature increased the size of the bonding neck, thus reducing porosity and improving mechanical properties. They also indicated that the estimated neck size was smaller than that observed in experiments, which could be attributed to the neglect of the gravitational effect and the erroneous assumption of a circular cross-section, whereas in reality, it was observed to be elliptical [49]. The aforementioned research assumed a uniform temperature distribution during the interfacial sintering process; however, in reality, the temperature distribution is non-uniform [152], as depicted in Fig. 7b. Therefore, combining the temperature distribution with the interfacial sintering models can improve the predictive accuracy.

### 3.2.2. Crystallization

Crystallization is a phenomenon in which polymer chains partially fold to form ordered lamellae [173]. When the temperature of the printed material cools between its melting point and its glass transition temperature, crystallization occurs in semi-crystalline thermoplastic resins [149,173]. Based on experimental observations [149,173,177, 178], an increase in the degree of crystallinity has a positive effect on the mechanical properties. Thus, increasing the degree of crystallinity is a well-adopted strategy to improve the mechanical properties of the printed parts. This can be achieved by slowing the cooling process [149, 177,178]. It is important to note that semi-crystalline thermoplastic resins are prone to significant shrinkage after cooling, due to the dense packing of polymer chains that occurs during crystallization [173]. Therefore, the degree of crystallinity should be carefully controlled to

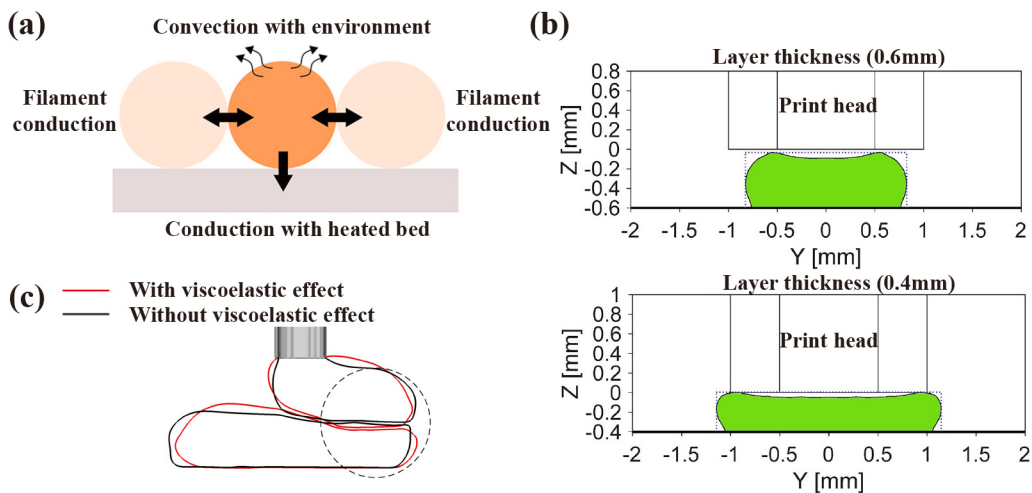


**Fig. 6.** (a) Heat transfer modes for 3D printing; (b) cross-sections of the deposited material with different layer thickness (adapted from [165]); (c) flow simulation of the deposition process with viscoelastic and without viscoelastic effect (reproduced from [166]). Adapted/reproduced with permission.

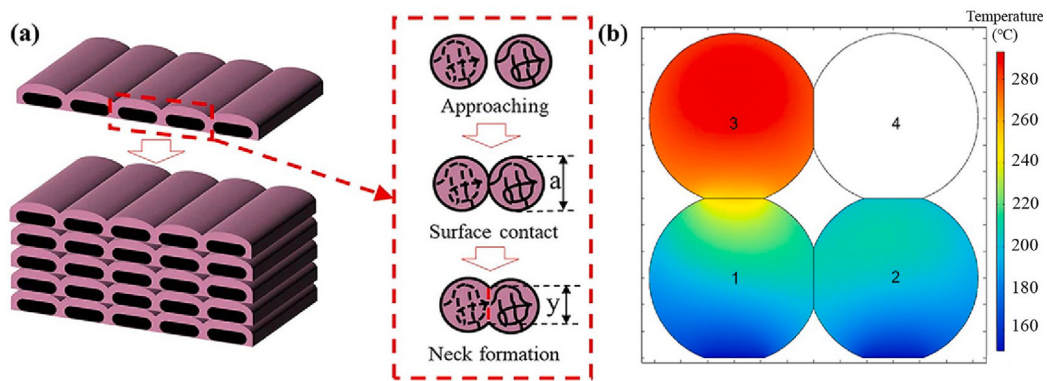


**Fig. 7.** (a) Formation process of the bonding neck during the CF3DP process ( $a$  represents the diameter of the printed filament and  $y$  represents the diameter of the bonding neck) [66]; (b) temperature distribution of filament cross-section during the CF3DP process (filaments 1–3 are active (deposited), while filament 4 is still inactive) [152,176]. Reproduced with permission.

ensure that the shrinkage of the printed parts aligns with the required dimensional precision [179].

Numerous models have been proposed for the study of crystallization kinetics, such as the Avrami model [38,130,180] under isothermal conditions and the Nakamura model under non-isothermal conditions [181]. These crystallization kinetic models provide predictions of the degree of crystallinity but fail to offer information on the evolution of crystallization morphology [182], which is notably correlated with the mechanical properties of the printed parts [183]. Moreover, in the CF3DP process, the presence of fiber leads to the formation of resin's transcrystallization on the fiber surface [184,185], which can effectively enhance the interfacial properties [174,186,187].

In order to elucidate the dynamic evolution of crystallization, several approaches — including molecular dynamics (MD) [45,188,189], pixel coloring [190,191], and phase field [192,193] — have been adopted to predict the crystallization kinetics and the morphology of semi-crystalline polymers [182]. Among them, the MD method can study the effects of micro-structure [189], temperature [47], and stretch [194] on the crystal nucleation from an atomic perspective. However, due to limitations in length [195] and time scales [196–198], the MD method cannot capture the entire formation process of crystalline structure [182]. The pixel coloring method is an alternative method to predict the crystallization morphology in resin. In this method, the simulation domain is divided into spatial pixels and different colors are assigned to these pixels to describe the crystal growth.

This growth initiates from a random nucleation center and expands along the radial direction, with the growth rate being determined by the crystallization kinetic models [190]. Besides, the phase field method is similar to the pixel coloring method but adopts the phase field equations to calculate the crystal growth rate based on the energy minimization principle [192,193].

### 3.2.3. Warpage

Warpage is a structural deformation caused by the accumulation of residual stress during the rapid heating and cooling cycles in the CF3DP process [35,36,101]. The residual stress is mainly induced by the non-uniform deformation due to the temperature gradient and crystallization morphology [35]. During the cooling process, there is a significant and non-uniform temperature gradient within the parts, which causes the inhomogeneous material contraction and the generation of residual stress. Furthermore, crystallization causes local volume shrinkage in the crystalline region, and this unbalanced structural deformation between the crystalline and non-crystalline regions can also generate residual stress [35,173]. Considering the effect of the temperature gradient, residual stress can be reduced by slowing down the cooling process and reducing the temperature gradient [36]. Auxiliary heating sources are usually used to slow the cooling process [102,199]. However, reducing the temperature gradient can promote crystallization, which in turn increases the accumulation of residual stress [35]. Therefore, balancing the temperature gradient and crystallization morphology is key to controlling warpage deformation.

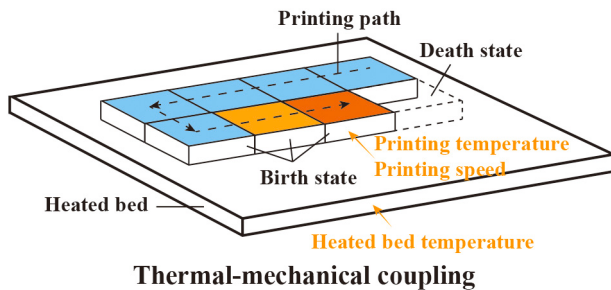


Fig. 8. The schematic diagram of birth-death element technique for 3D printing.

To control the cooling process and mitigate warpage deformation, it is imperative to optimize process parameters, such as the forming temperature and the printing speed, using numerical modeling. The most common approach is the so-called birth-death element technique [153–155]. This approach tracks the fiber path by assigning the corresponding elements to a birth state, which are then considered in the heat transfer calculation, as illustrated in Fig. 8. In this way, the evolution of temperature field during deposition is obtained, and the warpage deformation can be predicted through thermal-mechanical coupling [36]. It should be noted that for the CF3DP process, the fiber alters the thermal properties of the resin, which requires extra attention during modeling. Considering the material's anisotropy introduced by continuous fiber, Ghnatos et al. [36] simulated the deposition process of CF3DP and discovered that increasing the printing temperature and heated bed temperature led to a reduction in both the maximum deformation and residual stresses. It is worth noting that, as each deposited layer requires at least one element and given the small layer thickness relative to the part size, the simulation using the birth-death element technique requires a considerable number of elements, leading to a prohibitive computation time [36]. To increase computational efficiency, some researchers have employed the proper generalized decomposition technique, which uses independent meshes in the in-plane and out-of-plane directions [36,200].

### 3.2.4. Impregnation

Impregnation refers to the phenomenon in which molten resin infiltrates the continuous fiber bundle (Fig. 9). The impregnation phenomenon primarily occurs in the in-situ impregnation approach, as the prepreg used in the towpreg pultrusion approach has already been pre-impregnated. The continuous fiber bundle is composed of thousands of monofilaments, and its impregnation process can be considered as a problem of porous medium infiltration [49]. Effective impregnation can minimize the void content within the fiber bundle, thus greatly improving the mechanical properties of the composite [57]. Based on previous studies [52,55,57,82,201,202], impregnation within the nozzle is limited due to the high viscosity of thermoplastic resin, insufficient pressure, incomplete spread of the fiber bundle, and limited residence time of printing at the typical printing speeds. The main impregnation process occurs during the deposition process, where the nozzle provides an external compressive force to facilitate impregnation [43,49,52].

As the dry fiber bundle enters the nozzle, the molten resin coats its surface and impregnates its interior [82]. The fiber bundle is then pulled from the nozzle, completing the impregnation process under the pressure exerted by the nozzle [43,49]. The degree of impregnation is influenced by three key factors: the residence time in the nozzle, the forming pressure during deposition, and the resin viscosity. The residence time, which is related to the printing speed, should be long enough to ensure that the resin effectively coats the fiber bundle's surface and impregnates its interior [49,52,57,82,203,204]. The forming pressure, which is affected by the layer thickness, provides an external force that drives the resin into the fiber bundle [43,49].

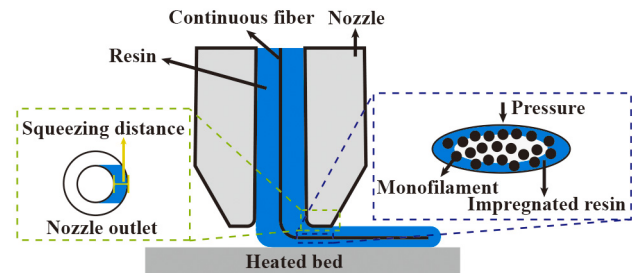


Fig. 9. Schematic diagram of fiber/matrix impregnation behavior during the CF3DP process.

The resin viscosity, which is determined by the printing temperature, should be low enough to reduce resistance during the impregnation process [43,49].

The impregnation process is commonly analyzed through Darcy's law [49,205,206], which characterizes the flow of molten resin through a porous medium. Because the fiber is coated by the molten resin, the resin flow along the axial direction of the fiber bundle is typically ignored and the model based on Darcy's law focuses on the resin flow along the radial direction [49]:

$$V_r = (K_r dp) / (\mu dr) \quad (2)$$

where,  $V_r$  is the impregnation velocity of the molten resin along the radial direction of the fiber bundle;  $\mu$  is the viscosity coefficient of the molten resin, which is closely related to the printing temperature and printing speed [49], and resin with lower viscosity is more accessible to impregnate into the fiber bundle;  $\frac{dp}{dr}$  is the pressure drop, which is associated with the forming pressure, and a higher value facilitates the resin impregnation into the fiber bundle; and  $K_r$  is the permeability, which is related to the distribution and volume fraction of monofilaments within the fiber bundle. Recent impregnation studies [39,49] of the CF3DP process have adopted the Gebart formula [207] to predict the permeability. However, due to its oversimplified consideration of the monofilament distribution, the Gebart formula cannot provide an accurate prediction of permeability [208]. Building upon this, many researchers have proposed more precise predictive models [209–211]. A detailed introduction to these models can be found in this review [208]. However, we would like to emphasize that the real impregnation process is influenced by complex phenomena [208], such as the capillary action and the fiber deformation induced by the CF3DP process. Therefore, it is best to determine the permeability value through experiments. The fundamental concept of permeability experiments involves measuring the pressure drop and the flow velocity variations as fluid flows through the porous medium, followed by calculating the permeability based on Darcy's law [212]. For the CF3DP process, we recommend two suitable experimental methods as references. Schell et al. [213] fixed a tensioned fiber bundle in a chamber with a flow channel and measured the transverse or longitudinal permeability by injecting liquid into one side of the fiber bundle. In the other method, Merhi et al. [214] employed a similar measurement approach, but designed a device that could compress the fiber bundle, allowing the measurement of permeability under compression.

The impregnation velocity can be calculated using Darcy's law and process parameters. By incorporating the printing time, the impregnation percentage can be estimated. Here, printing time generally refers to the ratio of the squeezing distance of nozzle (Fig. 9) to the printing speed. For example, with the combinations of printing speed, printing temperature, and layer thickness, Wang et al. [49] predicted the impregnation percentage and found that it increased with the elevated printing temperature, reduced printing speed, and decreased layer thickness. In addition, they found that when the impregnation percentage increased from 8% to 33%, the tensile strength improved

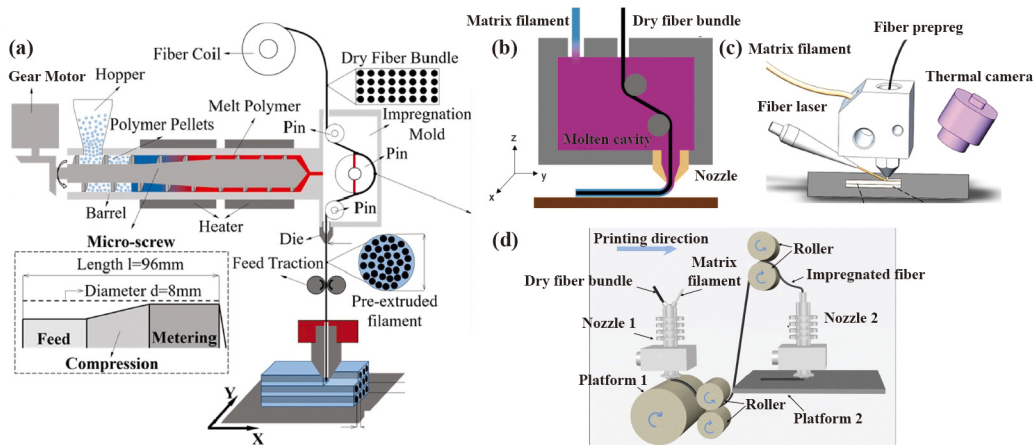


**Fig. 10.** Improved setups to enhance in-situ impregnation quality: (a) micro-screw in-situ impregnation CF3DP [57]; (b) pin-assisted in-situ impregnation CF3DP [202]; (c) laser-assisted in-situ impregnation CF3DP [82]; (d) two-stage in-situ impregnation CF3DP [216]. Reproduced with permission.

from 153.13 MPa to 221.78 MPa. Building upon this, Zhang et al. [39] introduced the temperature variation during the impregnation process into the model based on Darcy's law by accounting for changes in viscosity, and uncovered that a secondary impregnation during printing could be achieved by adopting the auxiliary laser heating. Furthermore, it is crucial to explore the dynamic evolution of the impregnation process, which can provide insight into the effects of micro attributes, such as surface tension and monofilament distribution [208,215]. This can be realized through the infiltration simulation of a porous medium, as reported in Ref. [215]. In the infiltration simulation of porous medium, the surface tension is introduced as an additional source term into the fluid momentum equation. Moreover, the distribution and content of monofilaments can be considered in a representative volume element (RVE) model, using the predictive models of permeability discussed above.

In addition to optimizing the process parameters through process modeling [39,49], several researchers have also improved the CF3DP equipment to tackle the issue of insufficient fiber/matrix impregnation. For instance, Liu et al. [57] combined a micro-screw extruder with the in-situ impregnation CF3DP (Fig. 10a). In this approach, the dry fiber bundle is first impregnated in an impregnation mold and then deposited onto the platform through a nozzle. In the impregnation mold, the fiber bundle spreads as it passes through the pins, and the micro-screw extruder provides sufficient pressure for impregnation. Combining both the effect of the pin and the micro-screw extruder, the impregnation can be significantly enhanced. Building upon this, An et al. [202] simplified the above equipment due to the complexity of the micro-screw extruder and proposed a pin-assisted printing method (Fig. 10b). This method directly embeds the pins from the impregnation mold into the molten cavity, utilizing the pins to spread the fiber bundle and improve the impregnation percentage. Furthermore, Luo et al. [82] and Zhang et al. [39] took a different approach by using the laser-assisted heating to increase the resin's flowability during the deposition process (Fig. 10c), thus promoting the fiber/matrix impregnation. Additionally, Wang et al. [216] developed a two-stage in-situ impregnation approach (Fig. 10d), in which one nozzle is used for initial impregnation and the impregnated fiber is transferred to another nozzle for printing. This approach provides additional printing pressure, further improving the impregnation percentage.

### 3.3. Discussion

This section offers a comprehensive review of research on the CF3DP process modeling, covering both the intra-nozzle and deposition processes. The CF3DP process is inherently complex, marked by a synergistic interplay among numerous process parameters and physical

phenomena that distinctly influence the quality of the printed parts. To facilitate reader understanding and reference, we have organized and summarized the main physical phenomena involved in the CF3DP process in Tables 3 and 4, along with the corresponding modeling methods and studies.

In summary, the studies mentioned above have independently modeled either the intra-nozzle process or the deposition process, without considering both simultaneously. As a result, deposition modeling typically assumes an idealized input material, neglecting the presence of bubbles within the molten resin and assuming a uniform flow rate and temperature. However, the accurate reproduction of the deposition process is heavily dependent on these input material properties, which are determined by the intra-nozzle process. Therefore, it is important to establish the connection between the modeling of the intra-nozzle and the deposition processes, and addressing the challenge of information exchange between the modeling of the two processes is crucial.

These process modeling methods reviewed in this section focus on the fundamental process mechanisms influenced by the process parameters; however, further effort is required to establish the relationship between the process mechanism and the mechanical properties as well as the failure behavior of the printed parts. We remark that during the analyses of mechanical properties and failure behavior, considering the effect of the manufacturing process is crucial, since the resultant defects and micro-structure significantly affect the service behavior of the printed products. In the following sections, we will discuss the modeling strategy, which analyzes the mechanical properties and failure behavior based on the outcomes of the process modeling.

## 4. Multiscale modeling and property evaluation

For CFRTPCs, the presence of multiple micro-structures results in a multiscale system, necessitating the consideration of multiscale properties in the structural design. Additionally, the manufacturing process involves a series of complex physical phenomena, requiring careful attention to the underlying micro-mechanisms, such as micro defect formation, phase transition, and impregnation (Fig. 11). Therefore, to achieve an optimized structural design and process parameter set, a modeling approach that includes multiscale properties and mechanisms is essential. In this section, we will discuss the different modeling techniques at both the macroscale and microscale, along with their coupling strategies. The focus and modeling methods are summarized at the end of this section, as presented in Table 5.

**Table 3**  
Physical phenomena and corresponding modeling methods involved in the intra-nozzle process.

| Phenomena                      | Focus                                 | Methods                   | References   |
|--------------------------------|---------------------------------------|---------------------------|--------------|
| Melt flow <sup>b</sup>         | Flow behavior of molten resin         | Bellini model             | [125]        |
|                                |                                       | Osswald model             | [126]        |
|                                |                                       | FVM                       | [38,129,130] |
|                                |                                       | SPH                       | [48]         |
| Fiber deformation <sup>b</sup> | Structural behavior of flexible fiber | FEM                       | [129,139]    |
|                                |                                       | DEM                       | [48]         |
| FSI <sup>b</sup>               | Interaction between resin and fiber   | Resin (FVM) + Fiber (FEM) | [129,139]    |
|                                |                                       | Resin (FVM) + Fiber (DEM) | [147]        |
|                                |                                       | Resin (SPH) + Fiber (DEM) | [48]         |

<sup>a</sup> Suitable for towpreg pultrusion approach.

<sup>b</sup> Suitable for in-situ impregnation approach.

**Table 4**  
Physical phenomena and corresponding modeling methods involved in the deposition process.

| Phenomena                            | Focus                      | Methods                    | References   |
|--------------------------------------|----------------------------|----------------------------|--------------|
| Interfacial sintering <sup>a,b</sup> | Interfacial strength       | Frenkel-based model        | [66,113,175] |
| Crystallization <sup>a,b</sup>       | Degree of crystallinity    | Avrami and Nakamura models | [38,180,181] |
|                                      | Crystallization morphology | MD                         | [47,189,194] |
|                                      |                            | Pixel coloring             | [190]        |
|                                      |                            | Phase field                | [192,193]    |
| Warpage <sup>a,b</sup>               | Residual stresses          | Birth-death element        | [36,154]     |
| Impregnation <sup>b</sup>            | Impregnation percentage    | Darcy's law                | [39,49]      |

<sup>a</sup> Suitable for towpreg pultrusion approach.

<sup>b</sup> Suitable for in-situ impregnation approach.

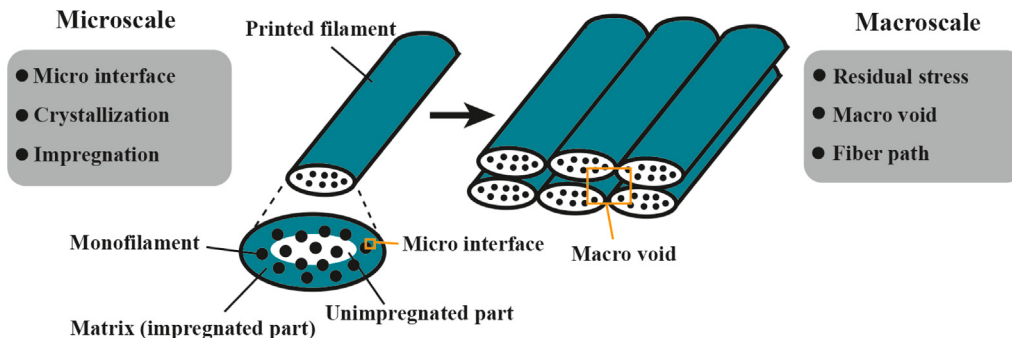


Fig. 11. The multiscale modeling schematic diagram of the CF3DP process.

#### 4.1. Macroscale modeling

Macroscale modeling concentrates on how the process parameters, such as forming temperature, printing speed, layer thickness, and fiber path, affect the final printed parts from a global perspective. In this case, the combined effect of the process parameters on the overall mechanical properties of the entire part can be analyzed through dynamic simulation of the temperature field variation [36,38]. With this varied temperature information, the residual stress can be evaluated, as it closely depends on the local volume shrinkage in the crystalline region and the mismatch of thermal expansion during the manufacturing process, as discussed in Section 3.2.3. Then, the residual stress, as a predefined field, can be used in the mechanical property evaluation of the printed parts [36]. In addition, the temperature variation also affects the flow behavior of the molten resin by altering its viscosity and phase state [38]. This results in changing size and proportion of macro voids between the printed filaments (Fig. 11), and a structural mechanics model can be established based on this morphology information to analyze the process effect on the mechanical properties [38].

These studies mainly analyze the mechanical properties by introducing process-related information from process modeling to structural mechanics evaluation. However, they usually ignore the effect of the fiber path, which plays a crucial role in the mechanical properties of the printed parts due to the anisotropic nature of continuous fiber [217].

By optimizing the fiber path based on the stress distribution, improved strength efficiency can be achieved [217–221]. Specifically, for lightweight CFRTPC applications, researchers have developed novel topology optimization methods to achieve structural design and fiber paths with improved performance while adhering to manufacturing constraints [222–224]. In these advanced structures, the fiber paths are more complex, and it is imperative to be considered in macroscale modeling. The commonly employed approaches to include the fiber path into the structural mechanics model are embedded elements (EE) [225, 226] and voxel modeling [227]. In the EE approach, the meshes of the resin and fiber components are generated independently, and the fiber mesh is embedded into the resin mesh by connecting their nodes through a weight function (Fig. 12a) [226]. However, there is an additional stiffness in the calculation due to the redundant resin volume at the fiber locations, which affects the computation accuracy [225]. This volume redundancy cannot be neglected in the case of a high fiber volume fraction, and in such instances, the voxel modeling method presents a viable alternative. As shown in Fig. 12b, the voxel modeling method includes the local orientation and volume fraction of fiber — extracted from each pixel in the pre-generated pixelated fiber path image — into the FEM element (voxel) by defining the anisotropic material properties [227].

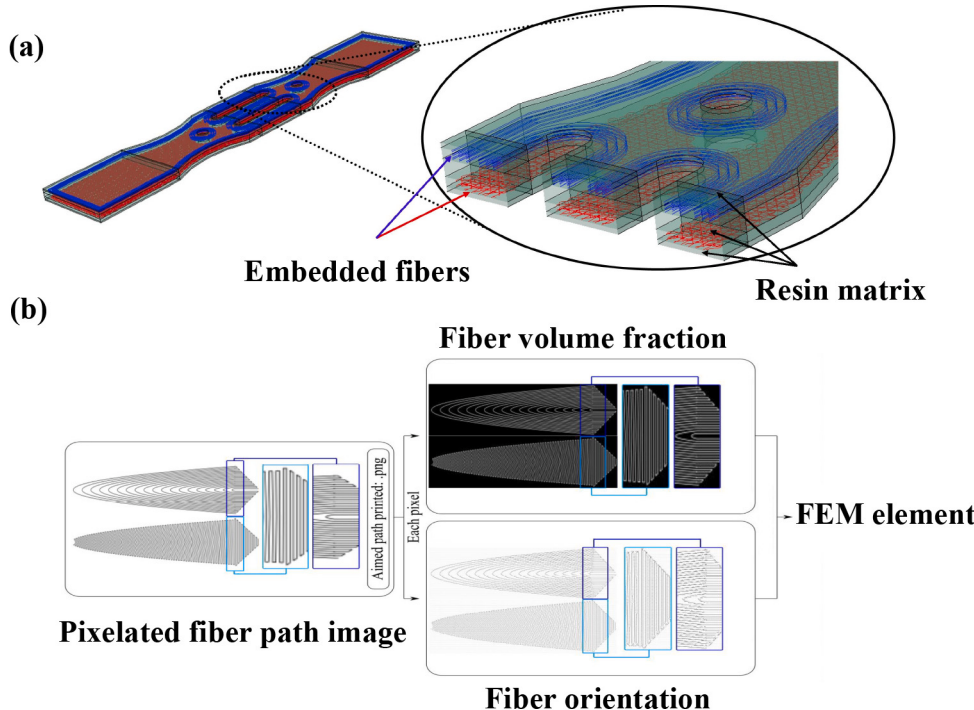


Fig. 12. (a) Schematic diagram of the EE technique [225]; (b) flow chart of the voxel modeling technique [227]. Reproduced with permission.

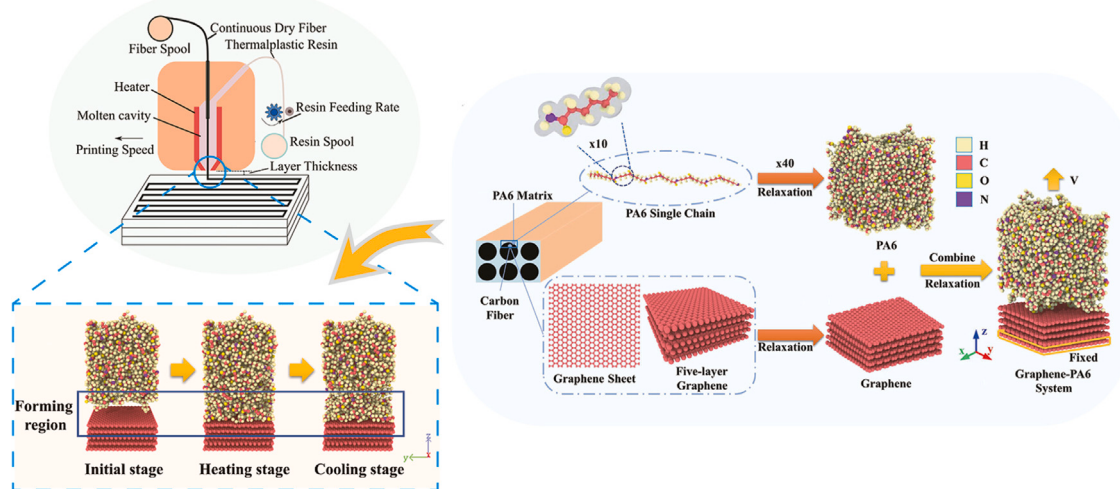


Fig. 13. Atomistic modeling of the continuous fiber 3D printing [45]. Reproduced with permission.

#### 4.2. Microscale modeling

Due to the limitations of the simulation system scale, the macroscale modeling cannot cover the process-related micro-structures and micro-mechanisms. CF3DP is a complicated process involving multiple physical mechanisms related to the formation of a series of micro-structures, such as the micro interface between fiber and resin, crystals within the resin, and impregnated structures within the fiber bundle. These micro-structures significantly affect the mechanical properties of the printed parts, and thus, it is imperative to include microscale modeling in the exploration of the process mechanism.

For the micro interface between fiber and resin, the MD method is typically used to mimic its dynamic formation process [45,228]. For example, Wang et al. [45] analyzed the effect of the printing temperature on the micro interface from an atomistic perspective (Fig. 13).

and highlighted that the elevated temperature promoted the bonding between the fiber and resin due to the intensified molecular thermal motion. The manufacturing process also affects the crystal growth, and in process modeling, this is evaluated through the degree of crystallinity and crystalline morphology, as discussed in Section 3.2.2. Based on the predicted degree of crystallinity, the resin properties can be calculated through the Voigt rule of mixtures, considering the properties of crystalline and amorphous phases [229]. Moreover, the effect of the crystalline morphology can be considered in an RVE model, which modifies the anisotropic properties of the corresponding elements based on the crystal orientation [230]. Similarly, the mechanical property evaluation of the impregnated structure can also be carried out based on the degree and morphology of impregnation (Fig. 11).

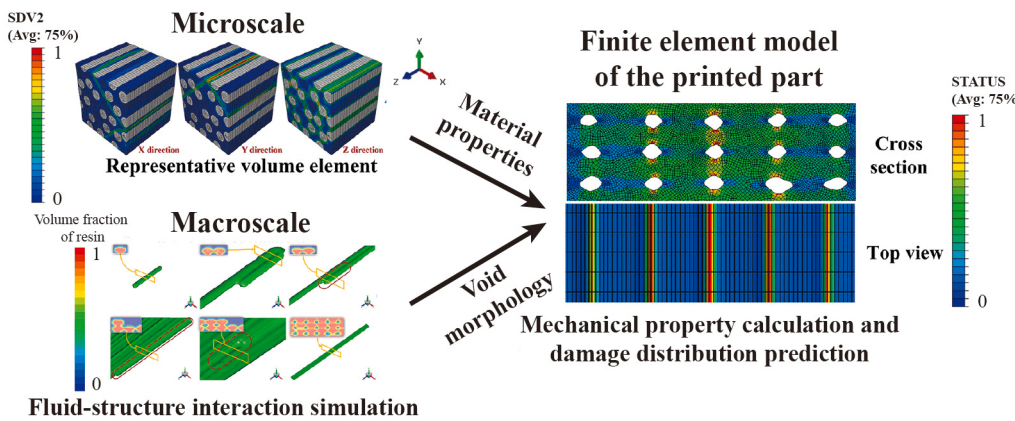


Fig. 14. The schematic diagram of multiscale fluid–structure interaction simulation of the CF3DP process [38]. Adapted with permission.

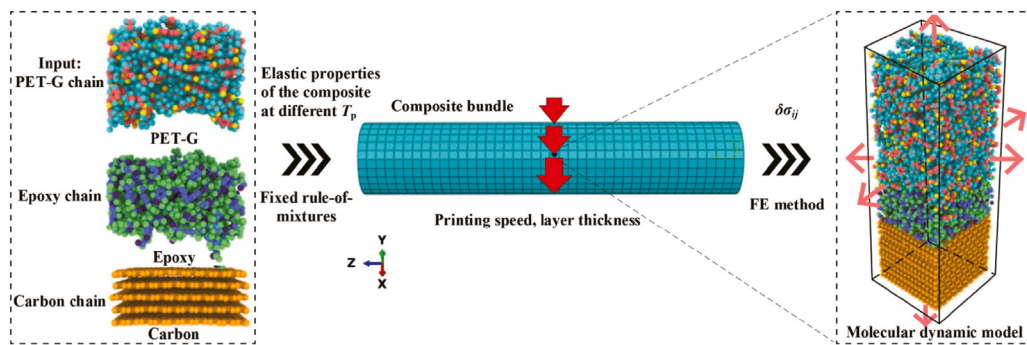


Fig. 15. Schematic diagram of parameter transfer in the multiscale approach for interfacial interaction [44]. Reproduced with permission.

#### 4.3. Multiscale coupling

Although microscale modeling can provide insight into the effect of the CF3DP process on the micro-structures within the printed parts, it cannot directly guide the process optimization due to limitations in size and time scale. Therefore, multiscale coupling between macroscale and microscale modeling is crucial. In this way, microscale modeling can modify the material properties and constitute relations, which serve as inputs for macroscale modeling. The combination of modeling approaches on these two scales has the potential to provide detailed analysis of the mechanical properties. For instance, Fu et al. [38] combined the calculated material properties from an RVE model — containing monofilaments and resin — with the predicted macro void morphology from a flow simulation, to evaluate the mechanical properties of the printed composites (Fig. 14). The process parameters were considered in the flow simulation [38].

Furthermore, as illustrated in Fig. 15, Liu et al. [44] utilized the MD method to predict the composite properties from the microscale, which were then introduced into a macro finite element model to capture the stress information, considering factors such as printing temperature, printing speed, and layer thickness. Then, this stress information was applied as the boundary condition for an MD model through the homogenization hypothesis, enabling the calculation of the interfacial bonding strength. Their results revealed that increasing the printing temperature and pressure was conducive to enhancing the interfacial bonding strength.

#### 5. Analysis of failure behavior

In engineering, the mechanical properties of products degrade upon failure, which significantly affects their continued serviceability. Failure is a localized phenomenon that typically initiates from defects

induced by the manufacturing process [231,232]. Therefore, the failure mode and location are closely related to the manufacturing process. It is imperative to take the manufacturing defects into account when performing a failure analysis. The following discussion will illustrate how these defects arise during the manufacturing process and their connection to the failure modes (as shown in Table 6).

CF3DP manufacturing defects consist of three types: fiber defects, matrix defects, and interfacial defects [233]. Regarding fiber defects, during the CF3DP process, the nozzle applies pressure to the filaments and spreads them in a transverse direction [234]. Since the CF3DP process cannot provide uniform tension and pressure control for continuous fiber [13], partial monofilaments in the fiber bundle may deviate from the intended printing trajectory, resulting in the fiber misalignment (Fig. 16a). The printed part tends to experience buckling failure in the misaligned regions under longitudinal compressive loads, due to the high shear stress concentrated in these regions [235]. Furthermore, the fiber is prone to misalignment, wrinkling, and folding (Fig. 16a) when printing with a large turning angle, due to the excessive drag force exerted by the nozzle, combined with the weak interfacial adhesion caused by the rapid cooling of the resin [13]. These defects damage the continuous fiber, potentially leading to fiber breakage and product failure [13]. To explore the relationship between the CF3DP process and fiber defects, Zhang et al. [13,236] studied the stress distribution of the fiber bundles at corners using the FE model, revealing that the fiber bundles were prone to defects at corners due to the nozzle dragging and weak interfacial bonding (Fig. 16b). This research primarily investigated how fiber defects relate to the printing trajectory and equipment. However, based on the model they developed, future research could explore how printing speed, printing temperature, and layer thickness affect the nozzle dragging force and interfacial adhesion. To incorporate fiber defects into failure analysis, some researchers [234,237–239] have believed that defects contribute to the

**Table 5**  
Modeling summary of the various scales.

| Scales     | Focus  | Methods   | References         |
|------------|--|---|--------------------|
| Macroscale | Residual stress & Macro void   | Combine simulated temperature variation with the material's thermal and flow behaviors                                  | [36,38]            |
|            | Fiber path   | EE<br>Voxel modeling  | [225,226]<br>[227] |
| Microscale | Micro interface  | MD  | [45,228]           |
|            | Crystallization & Impregnation   | Degree of crystallinity and impregnation with Voigt rule of mixtures & Crystalline and impregnation morphology with RVE | [229,230]          |
| Multiscale | Take modified material properties from microscale as inputs for macroscale | RVE (material property) + flow simulation (macro void morphology)   | [38]               |
|            |  | MD (micro interface) + FE (stress information under process)  | [44]               |

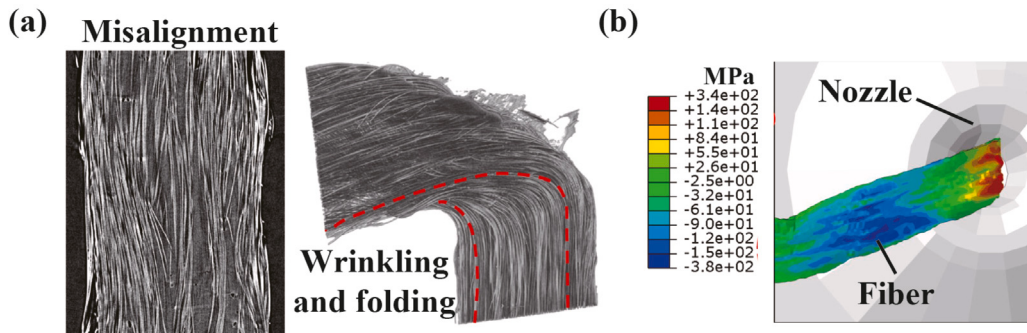


Fig. 16. (a) Micrographs of fiber misalignment, wrinkling, and folding defects [13]; (b) fiber misalignment simulation under the CF3DP process [13]. Adapted with permission.

degradation of material performance, ultimately leading to failure. Based on the concept of homogenization, researchers have integrated fiber defects — extracted from the corresponding micrographs — with micro-mechanical models to predict the constitutive behavior of the printed composites [234,237–239]. The predicted constitutive behavior is then applied in macroscopic FE simulations, combined with the experimentally derived failure criteria, to investigate the structural failure behavior [239].

Regarding matrix defects, void is the primary manufacturing defect, which can be classified into intra-bead and inter-bead voids (Fig. 17a) [233,240]. The intra-bead void is formed by the incomplete impregnation within the fiber bundle due to the limited printing time and pressure [39,49]. This void typically occurs in the in-situ impregnation approach, where impregnation occurs during printing [49]. The inter-bead void (macro void) results from the incomplete filling of the bead gaps by the resin, due to the rapid cooling of the resin and the limited nozzle pressure [38,241]. When the printed part is subjected to load, cracks initiate from the void defects and cause the matrix cracking, as illustrated in Fig. 17b. As the crack propagates, it overloads the adjacent fibers and ultimately leads to fiber breakage [23,75,240,242,243]. Void defects can be controlled by adjusting the process parameters [25,38] and stacking methods [38,75]. To explore the relationship between the process parameters and void defects, several researchers have studied the impregnation process in CF3DP based on Darcy's law [39,49]. Their findings suggested that the increased printing temperature and the reduced layer thickness positively affected the reduction of the intra-bead void (please refer to Section 3.2.4 for detailed content). Additionally, some scholars have employed the computational fluid dynamics to simulate the resin flow behavior during the CF3DP process [38]. They suggested that adopting a low printing speed and a staggered stacking method helped reduce the inter-bead voids. The above research focused on the flow behavior during the deposition process. However, as discussed in Section 3.1, the state of the melt as it exits the nozzle plays

a crucial role in the subsequent void filling. Therefore, establishing a simulation model that couples the flow behavior inside the nozzle and during the deposition process is of great significance for more accurate research on the void defect formation. Based on the calculated void defect information, the failure analyses have also been conducted. Some researchers have incorporated the void content as a correction parameter in the micro-mechanical models to predict the constitutive behavior of the printed composites [234,244–246], and subsequently investigated the failure behavior in conjunction with the failure criteria [237]. Moreover, some researchers have directly mapped the void morphology into the FE model to visually characterize the failure behavior caused by void defects (Fig. 14) [38].

Interfacial defects are generally classified into two types: fiber/matrix interface and inter-bead interface defects (Fig. 17a) [233]. When the printed part is being loaded, the interface acts as a bridge for load transfer between fibers [233]. A weak fiber/matrix interface may lead to fiber debonding from the resin, which is known as the fiber pull-out failure (Fig. 17c) [25]. Similarly, a weak inter-bead interface can cause delamination between the printed layers, resulting in the delamination failure (Fig. 17c) [25]. The primary causes of interfacial defects are uneven fiber wetting [233] and insufficient bonding between the printed beads [75], both of which result from the rapid cooling of the resin [75]. Recent studies have demonstrated that optimizing process parameters can effectively reduce the interfacial defects [25,44,45,66]. Many researchers have investigated the relationship between process parameters and inter-bead interface defects based on sintering models [66,113,152] (please refer to Section 3.2.1 for detailed content). However, due to the micron-scale diameter of the monofilament [249], research on the fiber/matrix interface defects remains limited. Wang et al. [45] utilized the MD method to simulate the formation process of the fiber/matrix interface and found that the interfacial properties improved with increasing printing temperature, leading to a shift in failure behavior from the interfacial failure to the resin cohesive

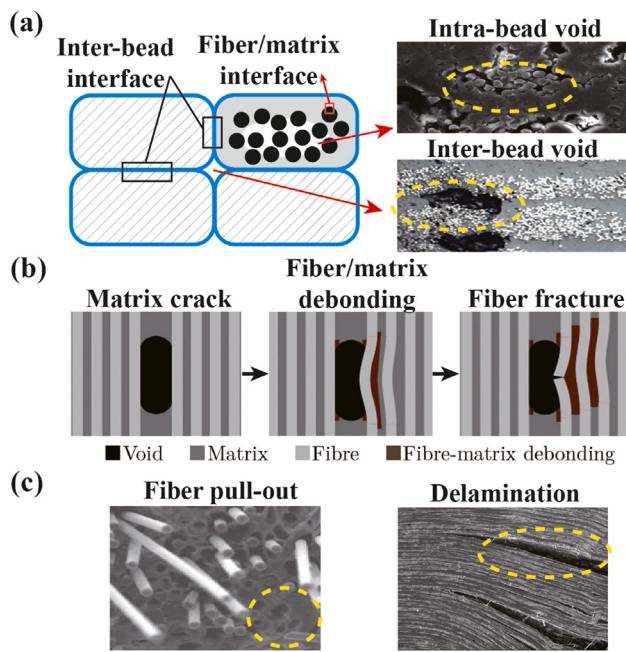


**Fig. 17.** (a) Matrix and interfacial defects manufactured by the CF3DP process [75, 247]; (b) schematic diagram of the void propagation [242]; (c) micrographs of the fiber pull-out and delamination failures [25, 248]. Adapted with permission.

failure. Moreover, Wang et al. [250] employed the MD method to study the interfacial delamination at the microscale and used the calculated constitutive relation as the input of cohesive zone modeling (a failure model of delamination) to analyze the interfacial failure at the macroscale. The aforementioned work provides a theoretical explanation for the fiber/matrix interfacial behavior, but it is limited by the computational scale and efficiency of the MD method [197, 251], which prevents accurate quantitative prediction of the interfacial performance. Recently, the development of coarse-grained MD methods [252] to expand the computational scale and enhanced sampling techniques [197, 251] to accelerate calculations may offer a solution to this challenge. Furthermore, to incorporate interfacial defects into the failure analysis, researchers have integrated the interfacial mechanical models into the FE model to simulate the interfacial failure [253, 254]. This interfacial mechanical model is typically configured based on the relationship between the interfacial separation force and the separation distance [253, 254], which can be modified based on the results of the process modeling.

The CF3DP process gives rise to a variety of manufacturing defects, resulting in a wide range of failure modes (as summarized in Table 6). Exploring the defect formation and the corresponding failure mechanisms is crucial for enhancing the service performance of the printed CFRTPCs and promoting their industrial application. In the field of traditional composite manufacturing processes, extensive research on defect formation and failure analysis has been conducted, offering well-established analytical theories and modeling methods. These approaches share similarities with the CF3DP process and may serve as valuable references, as detailed in these studies [231, 232, 255–260]. In the realm of the CF3DP process, although studies on defect formation mechanisms remain limited due to the novelty and complexity of the process, researchers have accumulated and summarized abundant experimental data on defect phenomena (as detailed in reviews [233, 261]). This growing body of knowledge is gradually shifting attention toward process modeling studies aimed at understanding and mitigating defect formation.

## 6. Emerging applications and challenges

With the advancement of the CF3DP process, increasing demands and challenges have emerged, including industrial, intelligent, and other novel applications. Addressing these critical issues is closely related to the development of high-precision and high-efficiency process modeling techniques. This section highlights these urgent challenges and discusses the essential role of process modeling in driving progress across these domains.

### 6.1. Industrial application

CF3DP technique enables the rapid fabrication of high-performance, lightweight, and complex structural components using the customized material selections. This unique capability makes it possible to fill the composite market gap between manual layup and large-scale manufacturing equipment. It is foreseeable that the industrial application of CF3DP will reduce the cost of composite products and accelerate their widespread adoption. Driven by this vision, efforts are being made to transition CF3DP from laboratory research to industrial application, although several critical challenges remain to be overcome, such as high-speed printing, large-scale printing, and arbitrary material printing.

The goal of high-speed printing is to improve the manufacturing efficiency, and achieving this requires the material extrusion rate to match the printing speed [262]. However, the traditional resistance heating method results in a low melting efficiency of the thermoplastic resin, which in turn limits the throughput of the printed material and restricts the printing speed [46, 263]. To increase the melting efficiency, advanced heating techniques have been introduced, such as screw extrusion [262], laser heating [46], and volumetric microwave heating [263]. These equipment modifications have introduced new process principles to the CF3DP process, necessitating an exploration of their process mechanisms. In this context, process modeling can provide preliminary guidance to help us quickly understand the new process mechanisms and determine the appropriate processing conditions, thereby accelerating the industrialization of the CF3DP technique.

The need for large-scale product manufacturing is increasing in industrial production. Previous research on CF3DP has primarily focused on small-scale structures, but there remains uncertainty regarding the successful expansion of this process to large-scale production. Recent research indicated that increasing the manufacturing size led to a significant decline in mechanical properties [264]. This decline may be attributed to the magnification of CF3DP-induced defects with the increased size, as a higher defect count markedly boosts the risk of structural failure. The insufficient forming pressure and rapid cooling in CF3DP result in weak interfaces and voids. To achieve large-scale printing, a pressing challenge is to reduce the number of manufacturing defects. A viable solution is to upgrade the CF3DP equipment by adding a pressure roller to increase the forming pressure and incorporating laser-assisted heating to enhance the interfacial bonding strength. Equipment upgrades require multiple iterative designs, and these modifications also introduce new process principles. Process modeling plays a vital role in exploring these novel process mechanisms and accelerating the iterative design of equipment.

In industrial production, the selection of suitable raw materials is typically guided by the requirements of product usage. Given that the range of materials available in industry is significantly broader than those typically studied in laboratories, there is a possibility of encountering raw materials that have not yet been researched. For such unexplored materials, we lack information on their process parameter values. However, in the context of efficient industrial production, it is impractical to start from scratch in exploring the forming process. Therefore, the challenge of arbitrary material printing lies in the rapid design of suitable process parameters. We remark that adopting a multiscale modeling approach to establish a mature and accurate CF3DP

**Table 6**

Failure modes and mechanisms caused by different manufacturing defects.

| Manufacturing defects  | Failure modes                      | Failure mechanisms   | References                     |
|--|------------------------------------|--|--------------------------------|
| Fiber defects<br>(misalignment, wrinkling, and folding)              | Fiber bulking;<br>Fiber breakage   | The shear stress concentrated at the defect region damages the fiber and causes the fiber bulking and breakage.  | [13,13,234–239]                |
| Matrix defects<br>(inter- and intra-bead voids)                      | Matrix cracking;<br>Fiber breakage | The crack initiates from the void and causes the matrix cracking. As the crack propagates, the overloading of adjacent fibers leads to the fiber breakage. | [38,39,49,234,<br>242,244–246] |
| Interfacial defects<br>(weak fiber/matrix and inter-bead interfaces) | Fiber pull-out;<br>Delamination    | The crack initiates at the weak interface and propagates until it leads to the fiber pull-out and delamination.  | [45,66,113,152,<br>250]        |

process model is a viable solution. A well-developed process model can rapidly predict the mechanical properties under different combinations of process parameters. Moreover, combining multiscale models with data-driven techniques can expedite the determination of the nonlinear relationship between process parameters and mechanical properties, thereby directly providing predictions of the recommended process parameter values based on actual performance requirements.

## 6.2. Intelligent application

Recent advancements in intelligent technologies have led to a significant revolution in the manufacturing field. Smart factories, driven by big data collection and analysis, are poised to replace the traditional factory model. The smart factory will intelligently determine the optimal manufacturing solutions and enable 24/7 automated production, thus greatly boosting the productivity of composite products. To achieve intelligent production in CF3DP, three major challenges need to be addressed: data collection through self-monitoring technology [265–267], data processing through data-driven technology [268–275], and intelligent production through digital twin technology [276, 277]. There are increasing requirements for the accuracy and efficiency of process modeling to promote the development of these intelligent technologies.

Self-monitoring is a technology that monitors the structural health of composite structures by utilizing their specific self-sensing features [265–267]. Self-monitoring can be realized through 3D printing due to its flexibility. For instance, the structural deformation can be measured based on the piezoresistive behavior of carbon fiber embedded in the printed parts [266]. The sensitivity, detection range, and cyclic stability of the self-monitoring structure are highly relevant to the material formulation and the precision of structural fabrication [267], which can be improved by revealing the underlying process mechanisms.

Data-driven technology employs intelligent algorithms to identify intricate nonlinear relationships [270–272]. Due to the complex nature of composite materials and manufacturing process, CF3DP entails handling extensive datasets throughout both the fabrication and service phases. These datasets encompass diverse material properties, controllable process parameters, and abundant structural health-monitoring information, which are collected through experiments and process modeling. To identify the relationships among these factors and benefit the process optimization, the data-driven techniques have been integrated into the CF3DP process [270–272]. In addition, by establishing a database comprising these collected data, the data-driven technique can also facilitate the real-time prediction of mechanical properties and failure behavior of the printed parts [273–275].

Furthermore, due to the remarkable diversity in structural designs and material properties as well as the susceptibility to defects, numerous trials are required when fabricating a new customized product, which hinders the widespread industrial application of CF3DP. The digital twin technology has emerged with the potential to reduce the trial tests, enhance the production efficiency, and improve the

mechanical property, thereby accelerating the industrial application of CF3DP. Digital twin enables the highly informative and scalable interaction between the physical objects and their virtual twins, which provides optimal process parameters during the fabrication phase and full life cycle monitoring of the printed products [276,277]. However, the digital twin relies on the high-fidelity virtual representation of the physical objects as well as the real-time updates between the physical objects and their virtual twins [276]. Both aspects are closely related to the process modeling and data-driven techniques, respectively. Therefore, to develop the digital twin of CF3DP and realize its widespread industrial application, more efforts should be devoted to improving process modeling and data-driven techniques.

## 6.3. Other novel application

In addition to the practical industrial application and forward-looking intelligent application, some scholars are exploring the utilization of CF3DP in special areas. For example, leveraging the flexibility advantage of CF3DP to fabricate three-dimensional spatial structures with unique mechanical properties, known as three-dimensional spatial printing [118,118,278–283]; incorporating a time dimension into CF3DP to print structures with specific functions, referred to 4D printing [284–288]; and exploring the manufacturing process of novel eco-friendly materials, known as eco-friendly 3D printing [201,289,290]. In this context, process modeling plays a crucial role in advancing the investigation of these pioneering applications.

Three-dimensional spatial printing refers to the complex part production of layers with three-dimensional characteristics. To meet the requirements of printing specific structures or to enhance performance in the thickness direction, it is sometimes necessary to print 3D layers. In recent years, many scholars have attempted to address this challenge from two aspects: equipment modification [118,278,279] and structural design [118,280–283]. Regarding equipment modification, given that the limited degrees of freedom in the equipment pose a major challenge to the three-dimensional spatial printing, some scholars have designed a two-nozzle printer [278]. One nozzle is designated for printing curved support structures of resin, while the other is used for printing curved layers of continuous fiber. Additionally, our team has conducted related work, developing six-axis desktop (Fig. 18a) [279] and robotic arm (Fig. 18b) [118] 3D printers. The enhanced degrees of freedom provide a foundation for achieving the spatial printing.

Regarding structural design, our team has designed a bidirectional sinusoidal curved structure suitable for CF3DP (Fig. 18c), which was inspired by the biological sinusoidal structure of *Odontodactylus scyllarus* [118,283]. During the printing process, we precisely controlled the resin feeding rate and continuously adjusted the nozzle orientation to ensure that the nozzle tip remained normal to the tangent plane of the fiber path, thereby achieving the printing of this three-dimensional curved structure. This structure can effectively enhance the load-bearing capacity along the thickness direction, with its impact strength showing an 80% improvement compared to the flat-layered structures. Furthermore, some scholars have developed a free-hanging

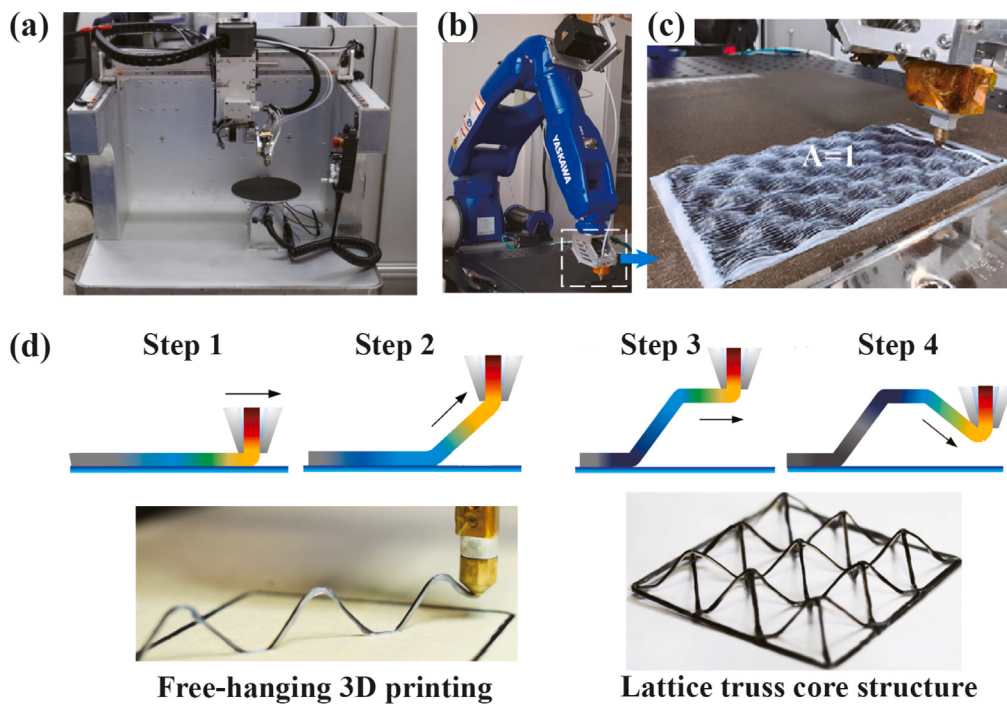


**Fig. 18.** (a) Six-axis desktop 3D printer [279]; (b) six-axis robotic arm 3D printer [118]; (c) the printing schematic diagram of the bidirectional sinusoidal curved structure [118]; (d) the schematic diagram of the free-hanging 3D printing [280]. Reproduced with permission.

3D printing technique capable of printing lattice truss core structures (Fig. 18d) [280–282]. They moved the nozzle in the three-dimensional space based on the lattice structure characteristics and accelerated the cooling process to solidify the thermoplastic resin, thereby preventing the printed structure from collapsing. This structure possesses superior specific compressive strength, potentially meeting the lightweight design demands. To achieve the printing of the aforementioned complex three-dimensional structures, precise process control is indispensable. Therefore, the process modeling methods discussed herein play a significant supportive role in advancing the development of three-dimensional spatial printing.

With the development of printing techniques and intelligent materials, 3D printing has evolved into 4D printing, which focuses on the manufacturing of intelligent composite parts. These parts can transform into a targeted morphology under external stimuli, such as heat, light, electricity, and magnetism [284–288]. The deformation behavior under external stimuli is typically predicted and programmed through the finite element model [291]. The controllable shape deformation is determined by the local material properties and the local geometric structures, both of which are closely related to the printing process [288,291]. For example, the accurate program of shape deformation can be realized by considering the influence of residual stress induced by the printing process on the deformation prediction model [291]. Moreover, the fiber path within the smart composite structure also affects its deformation behavior [292]. These studies emphasize the crucial role of process modeling, with its powerful capability to offer the process-related information critical for predicting the deformation behavior.

Eco-friendly 3D printing refers to the fabrication using novel eco-friendly materials. With the growing emphasis on sustainable development, the composite industry is gradually shifting toward utilizing recyclable thermoplastic resins and renewable biological materials [290, 293]. Due to its capabilities of cost-effectiveness and rapid manufacturing, CF3DP is typically employed to explore the mechanical behavior and processing knowledge of these new eco-friendly materials [201, 289,294]. For example, CF3DP was utilized to investigate the effectiveness of composite bone scaffolds composed of the biodegradable

continuous polyglycolic acid fiber and the poly ( $\epsilon$ -caprolactone) matrix [295,296]. However, unlike synthetic materials such as carbon fiber, biological materials are sensitive to temperature and moisture, making the printed parts more susceptible to processing conditions due to the high-temperature heating characteristic of CF3DP. For instance, due to the thermal degradation of the wood fiber, its strength decreases at elevated printing temperatures [297]. Additionally, high temperature can cause moisture loss in flax fiber, which results in reduced strength [298] and fiber shrinkage [294]. Consequently, the application of these green materials presents significant challenges for the process design of CF3DP, necessitating process modeling research to understand the fundamental mechanisms.

## 7. Conclusion

CF3DP represents huge potential to meet the growing demand for the rapid manufacture of CFRTPC products with complicated structures. To control manufacturing defects and improve the performance of the printed parts, process modeling is a powerful tool for optimizing the process parameters. Process modeling serves as a way to investigate the physical phenomena associated with the CF3DP process, establishing a connection between process parameters and printing performance. This paper summarizes the relevant literature on process modeling considering the intra-nozzle and deposition physical phenomena involved in the CF3DP process, including melt flow, fiber deformation, interfacial sintering, crystallization, warpage deformation, and impregnation. We also discuss how to integrate process modeling with property evaluation and failure analysis to identify the optimal processing window. Process modeling can also benefit the development of CF3DP in some innovative fields, such as industrial application, intelligent production, three-dimensional spatial printing, 4D printing, and eco-friendly 3D printing. However, with the involvement of new materials and new functional applications in CF3DP, a series of new challenges appear in process modeling. In our opinion, the multiscale modeling strategy, which can combine the advantages of models at various scales, will make a tremendous contribution to exploring the mechanisms underlying these challenges. Furthermore,

the combination of physics-based multiscale modeling with data-driven techniques is expected to be a key development trend in the future. This integration cannot only improve the prediction accuracy and efficiency, but also offer unique insights through intelligent algorithms. Given the promising prospects of process modeling, it is worth collective efforts in further research to unlock its full potential. With collective efforts, the maturation and broad application of CF3DP in various aspects of life could be realized.

### CRediT authorship contribution statement

**Shenru Wang:** Writing – review & editing, Writing – original draft, Methodology, Data curation, Conceptualization. **Xin Yan:** Writing – review & editing, Methodology, Funding acquisition, Conceptualization. **Baoning Chang:** Writing – review & editing. **Jiae Zhang:** Writing – review & editing, Formal analysis. **Siqin Liu:** Writing – review & editing, Data curation. **Fei Liu:** Writing – review & editing. **Junfan Shang:** Writing – review & editing. **Li-Hua Shao:** Resources, Funding acquisition. **Sha Yin:** Resources, Funding acquisition. **Wuxiang Zhang:** Writing – review & editing, Resources, Project administration, Funding acquisition, Conceptualization. **Yingdan Zhu:** Supervision, Resources, Project administration, Funding acquisition. **Xilun Ding:** Supervision, Resources.

### Declaration of competing interest

The authors declare that they have no known competing financial interests or personal relationships that could have appeared to influence the work reported in this paper.

### Acknowledgments

This work was supported by the National Natural Science Foundation of China (NSFC No. 12372106, No. 52205003, and No. 12272020), the Zhejiang Provincial Natural Science Foundation of China (LD22E050011), the Ningbo Key Research and Development Program, China (2022Z070, 2023Z054), the Opening Funding of State Key Laboratory of Structural Analysis for Industrial Equipment, Dalian University of Technology, China (No. GZ22101), and the Innovation Research Foundation of COMAC-BUAA Aircraft Research Institute, China (24010209). The authors acknowledge the support of the COMAC Beijing Aircraft Technology Research Institute. Shenru Wang acknowledges the insightful discussion with Fengtian Shi.

### References

- [1] Kwon D, Jang Y, Choi HH, Kim K, Kim G, Kong J, Nam SY, et al. Impacts of thermoplastics content on mechanical properties of continuous fiber-reinforced thermoplastic composites. Compos Part B Eng 2021;216:108859. <http://dx.doi.org/10.1016/j.compositesb.2021.108859>.
- [2] Zheng H, Zhang W, Li B, Zhu J, Wang C, Song G, Wu G, Yang X, Huang Y, Ma L. Recent advances of interphases in carbon fiber-reinforced polymer composites: A review. Compos Part B Eng 2022;233:109639. <http://dx.doi.org/10.1016/j.compositesb.2022.109639>.
- [3] Khan R. Fiber bridging in composite laminates: A literature review. Compos Struct 2019;229:111418. <http://dx.doi.org/10.1016/j.compstruct.2019.111418>.
- [4] Donough MJ, St John NA, Philips AW, Prusty BG, et al. Process modelling of in-situ consolidated thermoplastic composite by automated fibre placement—A review. Compos Part A Appl Sci Manuf 2022;163:107179. <http://dx.doi.org/10.1016/j.compositesa.2022.107179>.
- [5] Colombo C, Vergani L. Optimization of filament winding parameters for the design of a composite pipe. Compos Part B Eng 2018;148:207–16. <http://dx.doi.org/10.1016/j.compositesb.2018.04.056>.
- [6] Oromiehie E, Prusty BG, Compston P, Rajan G. Automated fibre placement based composite structures: Review on the defects, impacts and inspections techniques. Compos Struct 2019;224:110987. <http://dx.doi.org/10.1016/j.compstruct.2019.110987>.
- [7] Koon B, Stranberg N. Development and application of continuous fiber 3D printing process for aerospace. In: Int SAMPE tech conf. vol. 2021, 2021, p. 1223–34.
- [8] He X, Ding Y, Lei Z, Welch S, Zhang W, Dunn M, Yu K. 3D printing of continuous fiber-reinforced thermoset composites. Addit Manuf 2021;40:101921. <http://dx.doi.org/10.1016/j.addma.2021.101921>.
- [9] Kabir SF, Mathur K, Seyam A-FM. A critical review on 3D printed continuous fiber-reinforced composites: History, mechanism, materials and properties. Compos Struct 2020;232:111476. <http://dx.doi.org/10.1016/j.compstruct.2019.111476>.
- [10] Li N, Li Y, Liu S. Rapid prototyping of continuous carbon fiber reinforced polylactic acid composites by 3D printing. J Mater Process Technol 2016;238:218–25. <http://dx.doi.org/10.1016/j.jmatprotec.2016.07.025>.
- [11] Li N, Link G, Jelonnek J. 3D microwave printing temperature control of continuous carbon fiber reinforced composites. Compos Sci Technol 2020;187:107939. <http://dx.doi.org/10.1016/j.compscitech.2019.107939>.
- [12] Luan C, Yao X, Zhang C, Fu J, Wang B. Integrated self-monitoring and self-healing continuous carbon fiber reinforced thermoplastic structures using dual-material three-dimensional printing technology. Compos Sci Technol 2020;188:107986. <http://dx.doi.org/10.1016/j.compscitech.2019.107986>.
- [13] Zhang H, Chen J, Yang D. Fibre misalignment and breakage in 3D printing of continuous carbon fibre reinforced thermoplastic composites. Addit Manuf 2021;38:101775. <http://dx.doi.org/10.1016/j.addma.2020.101775>.
- [14] Qiao J, Li Y, Li L. Ultrasound-assisted 3D printing of continuous fiber-reinforced thermoplastic (FRTP) composites. Addit Manuf 2019;30:100926. <http://dx.doi.org/10.1016/j.addma.2019.100926>.
- [15] Chacón J, Caminero M, nez PN, García-Plaza E, García-Moreno I, Reverte J. Additive manufacturing of continuous fibre reinforced thermoplastic composites using fused deposition modelling: Effect of process parameters on mechanical properties. Compos Sci Technol 2019;181:107688. <http://dx.doi.org/10.1016/j.compscitech.2019.107688>.
- [16] Zhuo P, Li S, Ashcroft IA, Jones AI. Material extrusion additive manufacturing of continuous fibre reinforced polymer matrix composites: A review and outlook. Compos Part B Eng 2021;224:109143. <http://dx.doi.org/10.1016/j.compositesb.2021.109143>.
- [17] Goh GD, Yap YL, Agarwala S, Yeong WY. Recent progress in additive manufacturing of fiber reinforced polymer composite. Adv Mater Technol 2019;4(1):1800271. <http://dx.doi.org/10.1002/admt.201800271>.
- [18] Benamira M, Benhassine N, Ayad A, Dekhane A. Investigation of printing parameters effects on mechanical and failure properties of 3D printed PLA. Eng Fail Anal 2023;148:107218. <http://dx.doi.org/10.1016/j.englfailanal.2023.107218>.
- [19] Farrokhabadi A, Veisi H, Gharebaghi H, Montesano J, Behravesh AH, Hedayati SK. Investigation of the energy absorption capacity of foam-filled 3D-printed glass fiber reinforced thermoplastic auxetic honeycomb structures. Mech Adv Mater Struct 2023;30(4):758–69. <http://dx.doi.org/10.1080/15376494.2021.203919>.
- [20] Farrokhabadi A, Ashrafiyan MM, Behravesh AH, Hedayati SK. Assessment of fiber-reinforcement and foam-filling in the directional energy absorption performance of a 3D printed accordion cellular structure. Compos Struct 2022;297:115945. <http://dx.doi.org/10.1016/j.compstruct.2022.115945>.
- [21] Ning F, Cong W, Qiu J, Wei J, Wang S. Additive manufacturing of carbon fiber reinforced thermoplastic composites using fused deposition modeling. Compos Part B Eng 2015;80:369–78. <http://dx.doi.org/10.1016/j.compositesb.2015.06.013>.
- [22] Ning F, Cong W, Hu Y, Wang H. Additive manufacturing of carbon fiber-reinforced plastic composites using fused deposition modeling: Effects of process parameters on tensile properties. J Compos Mater 2017;51(4):451–62. <http://dx.doi.org/10.1177/0021998316646169>.
- [23] Goh GD, Dikshit V, Nagalingam AP, Goh GL, Agarwala S, Sing SL, Wei J, Yeong WY. Characterization of mechanical properties and fracture mode of additively manufactured carbon fiber and glass fiber reinforced thermoplastics. Mater Des 2018;137:79–89. <http://dx.doi.org/10.1016/j.matdes.2017.10.021>.
- [24] Prüss H, Vietor T. Design for fiber-reinforced additive manufacturing. J Mech Des 2015;137(11). <http://dx.doi.org/10.1115/1.4030993>.
- [25] Tian X, Liu T, Yang C, Wang Q, Li D. Interface and performance of 3D printed continuous carbon fiber reinforced PLA composites. Compos Part A Appl Sci Manuf 2016;88:198–205. <http://dx.doi.org/10.1016/j.compositesa.2016.05.032>.
- [26] Bettini P, Alitta G, Sala G, Di Landro L. Fused deposition technique for continuous fiber reinforced thermoplastic. J Mater Eng Perform 2017;26(2):843–8. <http://dx.doi.org/10.1007/s11665-016-2459-8>.
- [27] Mosleh N, Rezadoust AM, Darioush S. Determining process-window for manufacturing of continuous carbon fiber-reinforced composite using 3D-printing. Mater Manuf Process 2021;36(4):409–18. <http://dx.doi.org/10.1080/10426914.2020.1843664>.
- [28] Akhoundi B, Behravesh AH, Bagheri Saed A. An innovative design approach in three-dimensional printing of continuous fiber-reinforced thermoplastic composites via fused deposition modeling process: in-melt simultaneous impregnation. Proc Inst Mech Eng Part B J Eng Manuf 2020;234(1–2):243–59. <http://dx.doi.org/10.1177/0954405419843780>.

- [29] Zhang Y, Zhou J, Qin R, Shi S, Lu Y, Zhang X, Xu J, Chen B. Defect analysis and quality evaluation system for additive manufactured continuous fiber-reinforced polymer composites. *J Manuf Process* 2025;141:595–612. <http://dx.doi.org/10.1016/j.jmapro.2025.03.023>.
- [30] Liu F, Ferraris E, Ivens J. Mechanical investigation and microstructure performance of a two-matrix continuous carbon fibre composite fabricated by 3D printing. *J Manuf Process* 2022;79:383–93. <http://dx.doi.org/10.1016/j.jmapro.2022.04.050>.
- [31] Ye H, Mao P, He W, Li J, Dong Y, Wang X. Influence of process parameters on the tensile properties of CFRTP composites 3D printed structures. *Mech Adv Mater Struct* 2024;1–13. <http://dx.doi.org/10.1080/15376494.2024.2440632>.
- [32] Li H, Lou R, Liu B, Chen Y, Wang Y. Research on the fusion of continuous fiber reinforced thermoplastic filaments for fused filament fabrication. *Int J Solids Struct* 2023;276:112328. <http://dx.doi.org/10.1016/j.ijsolstr.2023.112328>.
- [33] Ueda M, Kishimoto S, Yamawaki M, Matsuzaki R, Todoroki A, Hirano Y, Le Duigou A. 3D compaction printing of a continuous carbon fiber reinforced thermoplastic. *Compos Part A Appl Sci Manuf* 2020;137:105985. <http://dx.doi.org/10.1016/j.compositesa.2020.105985>.
- [34] He Q, Wang H, Fu K, Ye L. 3D printed continuous CF/PA6 composites: Effect of microscopic voids on mechanical performance. *Compos Sci Technol* 2020;191:108077. <http://dx.doi.org/10.1016/j.compsitech.2020.108077>.
- [35] Samy AA, Golbang A, Harkin-Jones E, Archer E, Tormey D, McIlhagger A. Finite element analysis of residual stress and warpage in a 3D printed semi-crystalline polymer: Effect of ambient temperature and nozzle speed. *J Manuf Process* 2021;70:389–99. <http://dx.doi.org/10.1016/j.jmapro.2021.08.054>.
- [36] Ghanatos C, Fayazbakhsh K. Warping estimation of continuous fiber-reinforced composites made by robotic 3D printing. *Addit Manuf* 2022;55:102796. <http://dx.doi.org/10.1016/j.addma.2022.102796>.
- [37] Tuli NT, Khutun S, Rashid AB. Unlocking the future of precision manufacturing: A comprehensive exploration of 3D printing with fiber-reinforced composites in aerospace, automotive, medical, and consumer industries. *Heliyon* 2024;10(5):e27328. <http://dx.doi.org/10.1016/j.heliyon.2024.e27328>.
- [38] Fu Y, Yao X. Multi-scale analysis for 3D printed continuous fiber reinforced thermoplastic composites. *Compos Sci Technol* 2021;216:109065. <http://dx.doi.org/10.1016/j.compsitech.2021.109065>.
- [39] Zhang J, Yang W, Li Y. Process-dependent multiscale modeling for 3D printing of continuous fiber-reinforced composites. *Addit Manuf* 2023;73:103680. <http://dx.doi.org/10.1016/j.addma.2023.103680>.
- [40] Jiang X, Shan Z, Zang Y, Liu F, Wu X, Zou A, Liu X. Process optimization of continuous aramid fiber reinforced PA12 filaments and printed composites. *Polym Compos* 2024;45(15):13971–91. <http://dx.doi.org/10.1002/pc.28747>.
- [41] Almeida Jr JHS, Jayaprakash S, Kolari K, Kuva J, Kukko K, Partanen J. The role of printing parameters on the short beam strength of 3D-printed continuous carbon fibre reinforced epoxy-PETG composites. *Compos Struct* 2024;337:118034. <http://dx.doi.org/10.1016/j.comstruct.2024.118034>.
- [42] Zhu W, Zhi Q, Li D, Fu L, Zhang Z, Jiang C. Process-induced property loss of prepreg filaments with continuous fiber content of 65 vol% suitable for direct 3D printing. *J Manuf Process* 2024;131:1928–41. <http://dx.doi.org/10.1016/j.jmapro.2024.10.008>.
- [43] Zhang Z, Long Y, Yang Z, Fu K, Li Y. An investigation into printing pressure of 3D printed continuous carbon fiber reinforced composites. *Compos Part A Appl Sci Manuf* 2022;162:107162. <http://dx.doi.org/10.1016/j.compositesa.2022.107162>.
- [44] Liu F, Wang S, Zhang W, Ding X, Ferraris E, Ivens J. Mechanical and interfacial analysis of 3D-printed two-matrix continuous carbon fibre composites for enhanced structural performance. *Compos Part A Appl Sci Manuf* 2024;180:108105. <http://dx.doi.org/10.1016/j.compositesa.2024.108105>.
- [45] Wang S, Yan X, Chang B, Liu S, Shao L, Zhang W, Zhu Y, Ding X. Atomistic modeling of the effect of temperature on interfacial properties of 3D-printed continuous carbon fiber-reinforced polyamide 6 composite: From processing to loading. *ACS Appl Mater Interfaces* 2023;15(48):56454–63. <http://dx.doi.org/10.1021/acsami.3c12372>.
- [46] Tu Y, Tan Y, Zhang F, Zou S, Zhang J. High-throughput additive manufacturing of continuous carbon fiber-reinforced plastic by multifilament. *Polymers* 2024;16(5):704. <http://dx.doi.org/10.3390/polym16050704>.
- [47] Sigalas NI, Van Kraaij SA, Lyulin AV. Effect of temperature on flow-induced crystallization of isotactic polypropylene: A molecular-dynamics study. *Macromolecules* 2023;56(21):8417–27. <http://dx.doi.org/10.1021/acs.macromol.3c00916>.
- [48] Yang D, Wu K, Wan L, Sheng Y. A particle element approach for modelling the 3D printing process of fibre reinforced polymer composites. *J Manuf Mater Process* 2017;1(1):10. <http://dx.doi.org/10.3390/jmmp1010010>.
- [49] Wang F, Wang G, Ning F, Zhang Z. Fiber-matrix impregnation behavior during additive manufacturing of continuous carbon fiber reinforced polylactic acid composites. *Addit Manuf* 2021;37:101661. <http://dx.doi.org/10.1016/j.addma.2020.101661>.
- [50] Akhouni B, Nabipour M, Kordi O, Hajami F. Calculating printing speed in order to correctly print PLA/continuous glass fiber composites via fused filament fabrication 3D printer. *J Thermoplast Compos Mater* 2023;36(1):162–81. <http://dx.doi.org/10.1177/0892705721997534>.
- [51] Krajangwasdi N, Blok LG, Hamerton I, Longana ML, Woods BK, Ivanov DS. Fused deposition modelling of fibre reinforced polymer composites: a parametric review. *J Compos Sci* 2021;5(1):29. <http://dx.doi.org/10.3390/jcs5010029>.
- [52] Hu Q, Duan Y, Zhang H, Liu D, Yan B, Peng F. Manufacturing and 3D printing of continuous carbon fiber prepreg filament. *J Mater Sci* 2018;53(3):1887–98. <http://dx.doi.org/10.1007/s10853-017-1624-2>.
- [53] Dou H, Cheng Y, Ye W, Zhang D, Li J, Miao Z, Rudykh S. Effect of process parameters on tensile mechanical properties of 3D printing continuous carbon fiber-reinforced PLA composites. *Materials* 2020;13(17):3850. <http://dx.doi.org/10.3390/ma13173850>.
- [54] Hou Z, Tian X, Zhang J, Li D. 3D printed continuous fibre reinforced composite corrugated structure. *Compos Struct* 2018;184:1005–10. <http://dx.doi.org/10.1016/j.compstruct.2017.10.080>.
- [55] Chen K, Yu L, Cui Y, Jia M, Pan K. Optimization of printing parameters of 3D-printed continuous glass fiber reinforced polylactic acid composites. *Thin Wall Struct* 2021;164:107717. <http://dx.doi.org/10.1016/j.tws.2021.107717>.
- [56] Matsuzaki R, Ueda M, Namiki M, Jeong T-K, Asahara H, Horiguchi K, Nakamura T, Todoroki A, Hirano Y. Three-dimensional printing of continuous-fiber composites by in-nozzle impregnation. *Sci Rep* 2016;6(1):1–7. <http://dx.doi.org/10.1038/srep23058>.
- [57] Liu T, Tian X, Zhang Y, Cao Y, Li D. High-pressure interfacial impregnation by micro-screw in-situ extrusion for 3D printed continuous carbon fiber reinforced nylon composites. *Compos Part A Appl Sci Manuf* 2020;130:105770. <http://dx.doi.org/10.1016/j.compositesa.2020.105770>.
- [58] Hou Z, Tian X, Zhang J, Zhe L, Zheng Z, Li D, Malakhov AV, Polilov AN. Design and 3D printing of continuous fiber reinforced heterogeneous composites. *Compos Struct* 2020;237:111945. <http://dx.doi.org/10.1016/j.compstruct.2020.111945>.
- [59] Quan C, Han B, Hou Z, Zhang Q, Tian X, Lu TJ. 3D printed continuous fiber reinforced composite auxetic honeycomb structures. *Compos Part B Eng* 2020;187:107858. <http://dx.doi.org/10.1016/j.compositesb.2020.107858>.
- [60] Luo M, Tian X, Shang J, Yun J, Zhu W, Li D, Qin Y. Bi-scale interfacial bond behaviors of CCF/PEEK composites by plasma-laser cooperatively assisted 3D printing process. *Compos Part A Appl Sci Manuf* 2020;131:105812. <http://dx.doi.org/10.1016/j.compositesa.2020.105812>.
- [61] Stepanashkin A, Chukov D, Senatov F, Salimon A, Korsunsky A, Kaloshkin S. 3D-printed PEEK-carbon fiber (CF) composites: Structure and thermal properties. *Compos Sci Technol* 2018;164:319–26. <http://dx.doi.org/10.1016/j.compsitech.2018.05.032>.
- [62] Liu T, Tian X, Zhang M, Abliz D, Li D, Ziegmann G. Interfacial performance and fracture patterns of 3D printed continuous carbon fiber with sizing reinforced PA6 composites. *Compos Part A Appl Sci Manuf* 2018;114:368–76. <http://dx.doi.org/10.1016/j.compositesa.2018.09.001>.
- [63] Geng P, Zhao J, Wu W, Ye W, Wang Y, Wang S, Zhang S. Effects of extrusion speed and printing speed on the 3D printing stability of extruded PEEK filament. *J Manuf Process* 2019;37:266–73. <http://dx.doi.org/10.1016/j.jmapro.2018.11.023>.
- [64] Sabyrov N, Abilgaziyev A, Ali M, et al. Enhancing interlayer bonding strength of FDM 3D printing technology by diode laser-assisted system. *Int J Adv Manuf Technol* 2020;108(1):603–11. <http://dx.doi.org/10.1007/s00170-020-05455-y>.
- [65] Sanatgar RH, Campagne C, Nierstrasz V. Investigation of the adhesion properties of direct 3D printing of polymers and nanocomposites on textiles: Effect of FDM printing process parameters. *Appl Surf Sci* 2017;403:551–63. <http://dx.doi.org/10.1016/j.apsusc.2017.01.112>.
- [66] Fan C, Shan Z, Zou G, Zhan L, Yan D. Interfacial bonding mechanism and mechanical performance of continuous fiber reinforced composites in additive manufacturing. *Chin J Mech Eng* 2021;34(1):1–11. <http://dx.doi.org/10.1186/s10033-021-00538-7>.
- [67] Reverte JM, Caminero MÁ, Chacón JM. Mechanical and geometric performance of PLA-based polymer composites processed by the fused filament fabrication additive manufacturing technique. *Materials* 2020;13(8):1924. <http://dx.doi.org/10.3390/ma13081924>.
- [68] Tognana S, Frosinini C, Montecinos S. Influence of bed temperature on the final properties of PLA parts manufactured by material extrusion. *Rapid Prototyp J* 2024. <http://dx.doi.org/10.1108/RPJ-08-2024-0323>.
- [69] Han P, Tofangchi A, Zhang S, Izquierdo JJ, Hsu K. Interface healing between adjacent tracks in fused filament fabrication using in-process laser heating. *3D Print Addit Manuf* 2023;10(4):808–15. <http://dx.doi.org/10.1089/3dp.2022.0127>.
- [70] Prusinowski A, Kaczyński R. Tribological behaviour of additively manufactured fiber-reinforced thermoplastic composites in various environments. *Polymers* 2020;12(7):1551. <http://dx.doi.org/10.3390/polym12071551>.
- [71] Mishra V, Roy CK, Negi S, Kar S, Borah LN. 3D printing with recycled ABS resin: Effect of blending and printing temperature. *Mater Chem Phys* 2023;309:128317. <http://dx.doi.org/10.1016/j.matchemphys.2023.128317>.
- [72] Choi Y-H, Kim C-M, Jeong H-S, Youn J-H. Influence of bed temperature on heat shrinkage shape error in FDM additive manufacturing of the ABS-engineering plastic. *World J Eng Technol* 2016;4(3):186–92. <http://dx.doi.org/10.4236/wjet.2016.43D022>.

- [73] Ramian J, Ramian J, Dziob D. Thermal deformations of thermoplast during 3D printing: warping in the case of ABS. *Materials* 2021;14(22):7070. <http://dx.doi.org/10.3390/ma14227070>.
- [74] Mohammadzadeh M, Imeri A, Fidan I, Elkelany M. 3D printed fiber reinforced polymer composites-structural analysis. *Compos Part B Eng* 2019;175:107112. <http://dx.doi.org/10.1016/j.compositesb.2019.107112>.
- [75] Blok LG, Longana ML, Yu H, Woods BK. An investigation into 3D printing of fibre reinforced thermoplastic composites. *Addit Manuf* 2018;22:176–86. <http://dx.doi.org/10.1016/j.addma.2018.04.039>.
- [76] Dickson AN, Barry JN, McDonnell KA, Dowling DP. Fabrication of continuous carbon, glass and Kevlar fibre reinforced polymer composites using additive manufacturing. *Addit Manuf* 2017;16:146–52. <http://dx.doi.org/10.1016/j.addma.2017.06.004>.
- [77] Kumar R, Ranjan N. Influences of infill percentage, bed temperature and outer perimeters on elongation of 3D printed nylon 6. *Mater Today Proc* 2022;48:1661–5. <http://dx.doi.org/10.1016/j.mtpr.2021.09.529>.
- [78] Boparai K, Singh R, Fabbrocino F, Fraternali F. Thermal characterization of recycled polymer for additive manufacturing applications. *Compos Part B Eng* 2016;106:42–7. <http://dx.doi.org/10.1016/j.compositesb.2016.09.009>.
- [79] Vasanthkumar P, Balasundaram R, Senthilkumar N, Palanikumar K, Lenin K, Deepanraj B. Thermal and thermo-mechanical studies on seashell incorporated Nylon-6 polymer composites. *J Mater Res Technol* 2022;21:3154–68. <http://dx.doi.org/10.1016/j.jmrt.2022.10.117>.
- [80] Luo M, Tian X, Zhu W, Li D. Controllable interlayer shear strength and crystallinity of PEEK components by laser-assisted material extrusion. *J Mater Res* 2018;33(11):1632–41. <http://dx.doi.org/10.1557/jmr.2018.131>.
- [81] Pilipaka A, Gide KM, Beheshti A, Bagheri ZS. Effect of 3D printing process parameters on surface and mechanical properties of FFF-printed PEEK. *J Manuf Process* 2023;85:368–86. <http://dx.doi.org/10.1016/j.jmapro.2022.11.057>.
- [82] Luo M, Tian X, Shang J, Zhu W, Li D, Qin Y. Impregnation and interlayer bonding behaviours of 3D-printed continuous carbon-fiber-reinforced poly-ether-ether-ketone composites. *Compos Part A Appl Sci Manuf* 2019;121:130–8. <http://dx.doi.org/10.1016/j.compositesa.2019.03.020>.
- [83] Gupta A, Fidan I, Hasanov S, Nasirov A. Processing, mechanical characterization, and micrography of 3D-printed short carbon fiber reinforced polycarbonate polymer matrix composite material. *Int J Adv Manuf Technol* 2020;107:3185–205. <http://dx.doi.org/10.1007/s00170-020-05195-z>.
- [84] Vidakis N, Petousis M, Kechagias J. A comprehensive investigation of the 3D printing parameters' effects on the mechanical response of polycarbonate in fused filament fabrication. *Prog Addit Manuf* 2022;7(4):713–22. <http://dx.doi.org/10.1007/s40964-021-00258-3>.
- [85] Vidakis N, Petousis M, Korlos A, Velidakis E, Mountakis N, Charou C, Myftari A. Strain rate sensitivity of polycarbonate and thermoplastic polyurethane for various 3D printing temperatures and layer heights. *Polymers* 2021;13(16):2752. <http://dx.doi.org/10.3390/polym13162752>.
- [86] Park SJ, Lee JE, Lee HB, Park J, Lee N-K, Son Y, Park S-H. 3D printing of bio-based polycarbonate and its potential applications in ecofriendly indoor manufacturing. *Addit Manuf* 2020;31:100974. <http://dx.doi.org/10.1016/j.addma.2019.100974>.
- [87] Bakır AA, Atik R, Özerenç S. Effect of fused deposition modeling process parameters on the mechanical properties of recycled polyethylene terephthalate parts. *J Appl Polym Sci* 2021;138(3):49709. <http://dx.doi.org/10.1002/app.49709>.
- [88] Van de Voorde B, Katalagarianakis A, Huysman S, Toncheva A, Raquez J-M, Duretek I, Holzer C, Cardon L, Bernaerts KV, Van Hemelrijck D, et al. Effect of extrusion and fused filament fabrication processing parameters of recycled poly (ethylene terephthalate) on the crystallinity and mechanical properties. *Addit Manuf* 2022;50:102518. <http://dx.doi.org/10.1016/j.addma.2021.102518>.
- [89] Bhandari S, Lopez-Anido RA, Gardner DJ. Enhancing the interlayer tensile strength of 3D printed short carbon fiber reinforced PETG and PLA composites via annealing. *Addit Manuf* 2019;30:100922. <http://dx.doi.org/10.1016/j.addma.2019.100922>.
- [90] Hsueh M-H, Lai C-J, Wang S-H, Zeng Y-S, Hsieh C-H, Pan C-Y, Huang W-C. Effect of printing parameters on the thermal and mechanical properties of 3d-printed pla and petg, using fused deposition modeling. *Polymers* 2021;13(11):1758. <http://dx.doi.org/10.3390/polym13111758>.
- [91] Bembeneck M, Kowalski Ł, Kosof-Schab A. Research on the influence of processing parameters on the specific tensile strength of FDM additive manufactured PET-G and PLA materials. *Polymers* 2022;14(12):2446. <http://dx.doi.org/10.3390/polym14122446>.
- [92] Guessasma S, Belhabib S, Nouri H. Printability and tensile performance of 3D printed polyethylene terephthalate glycol using fused deposition modelling. *Polymers* 2019;11(7):1220. <http://dx.doi.org/10.3390/polym11071220>.
- [93] Sánchez DM, de la Mata M, Delgado FJ, Casal V, Molina SI. Development of carbon fiber acrylonitrile styrene acrylate composite for large format additive manufacturing. *Mater Des* 2020;191:108577. <http://dx.doi.org/10.1016/j.matdes.2020.108577>.
- [94] El Magri A, Ouassil S-E, Vaudreuil S. Effects of printing parameters on the tensile behavior of 3D-printed acrylonitrile styrene acrylate (ASA) material in Z direction. *Polym Eng Sci* 2022;62(3):848–60. <http://dx.doi.org/10.1002/pen.25891>.
- [95] Hameed AZ, Aravind Raj S, Kandasamy J, Shahzad MA, Baghdadi MA. 3D printing parameter optimization using taguchi approach to examine acrylonitrile styrene acrylate (ASA) mechanical properties. *Polymers* 2022;14(16):3256. <http://dx.doi.org/10.3390/polym14163256>.
- [96] Guessasma S, Belhabib S, Nouri H. Microstructure, thermal and mechanical behavior of 3D printed acrylonitrile styrene acrylate. *Macromol Mater Eng* 2019;304(7):1800793. <http://dx.doi.org/10.1002/mame.201800793>.
- [97] Bertolino M, Battegazzore D, Arrigo R, Frache A. Designing 3D printable polypropylene: Material and process optimisation through rheology. *Addit Manuf* 2021;40:101944. <http://dx.doi.org/10.1016/j.addma.2021.101944>.
- [98] Chatterjee R, Touhid SM, Chanda J, Acharya S, Basu D, Ghosh P, Mukhopadhyay R, Bandyopadhyay A. How open-stage melt crystallization affects tensile and shrinkage properties of 3D printed polypropylene. *Polym Eng Sci* 2023;63(9):2985–98. <http://dx.doi.org/10.1002/pen.26422>.
- [99] Kristiawan RB, Rusdyanto B, Imaduddin F, Ariawan D. Glass powder additive on recycled polypropylene filaments: A sustainable material in 3D printing. *Polymers* 2021;14(1):5. <http://dx.doi.org/10.3390/polym14010005>.
- [100] Spoerl M, Holzer C, Gonzalez-Gutierrez J. Material extrusion-based additive manufacturing of polypropylene: A review on how to improve dimensional inaccuracy and warpage. *J Appl Polym Sci* 2020;137(12):48545. <http://dx.doi.org/10.1002/app.48545>.
- [101] Casavola C, Cazzato A, Moramarco V, Pappalettera G. Residual stress measurement in fused deposition modelling parts. *Polym Test* 2017;58:249–55. <http://dx.doi.org/10.1016/j.polymertesting.2017.01.003>.
- [102] Spoerl M, Gonzalez-Gutierrez J, Sapkota J, Schuschnigg S, Holzer C. Effect of the printing bed temperature on the adhesion of parts produced by fused filament fabrication. *Plast Rubber Compos* 2018;47(1):17–24. <http://dx.doi.org/10.1080/14658011.2017.1399531>.
- [103] Wijnen B, Sanders P, Pearce JM. Improved model and experimental validation of deformation in fused filament fabrication of polylactic acid. *Prog Addit Manuf* 2018;3:193–203. <http://dx.doi.org/10.1007/s40964-018-0052-4>.
- [104] Snapp KL, Gongora AE, Brown KA. Increasing throughput in fused deposition modeling by modulating bed temperature. *J Manuf Sci Eng* 2021;143(9):094502. <http://dx.doi.org/10.1115/1.4050177>.
- [105] Nakagawa Y, Mori K-i, Yoshino M. Laser-assisted 3D printing of carbon fibre reinforced plastic parts. *J Manuf Process* 2022;73:375–84. <http://dx.doi.org/10.1016/j.jmapro.2021.11.025>.
- [106] Yao J, Duongthipthewa A, Xu X, Liu M, Xiong Y, Zhou L. Interlayer bonding improvement of PEEK and CF-PEEK composites with laser-assisted fused deposition modeling. *Compos Commun* 2024;45:101819. <http://dx.doi.org/10.1016/j.coco.2024.101819>.
- [107] Han P, Torabnia S, Riyad MF, Thippanna V, Song K, Hsu K. In-process laser heating for mechanical strength improvement of FFF-printed PEEK. *Prog Addit Manuf* 2024;1–10. <http://dx.doi.org/10.1007/s40964-024-00833-4>.
- [108] Bräuer G, Sachsenhofer K, Lang RW. Material and process engineering aspects to improve the quality of the bonding layer in a laser-assisted fused filament fabrication process. *Addit Manuf* 2021;46:102105. <http://dx.doi.org/10.1016/j.addma.2021.102105>.
- [109] Ravi AK, Deshpande A, Hsu KH. An in-process laser localized pre-deposition heating approach to inter-layer bond strengthening in extrusion based polymer additive manufacturing. *J Manuf Process* 2016;24:179–85. <http://dx.doi.org/10.1016/j.jmapro.2016.08.007>.
- [110] Du J, Wei Z, Wang X, Wang J, Chen Z. An improved fused deposition modeling process for forming large-size thin-walled parts. *J Mater Process Technol* 2016;234:332–41. <http://dx.doi.org/10.1016/j.jmatprotec.2016.04.005>.
- [111] Yiwen T, Yuegang T, Fan Z, Jun Z. Laser assisted rapid 3D printing of continuous carbon fiber reinforced plastics: Simulation, characterization, and properties. *Polym Compos* 2023;44(6):3084–94. <http://dx.doi.org/10.1002/pc.27303>.
- [112] Le Dugou A, Chabaud G, Matsuzaki R, Castro M. Tailoring the mechanical properties of 3D-printed continuous flax/PLA biocomposites by controlling the slicing parameters. *Compos Part B Eng* 2020;203:108474. <http://dx.doi.org/10.1016/j.compositesb.2020.108474>.
- [113] Garzon-Hernandez S, Garcia-Gonzalez D, Jérusalem A, Arias A. Design of FDM 3D printed polymers: An experimental-modelling methodology for the prediction of mechanical properties. *Mater Des* 2020;188:108414. <http://dx.doi.org/10.1016/j.matdes.2019.108414>.
- [114] Ming Y, Zhang S, Han W, Wang B, Duan Y, Xiao H. Investigation on process parameters of 3D printed continuous carbon fiber-reinforced thermosetting epoxy composites. *Addit Manuf* 2020;33:101184. <http://dx.doi.org/10.1016/j.addma.2020.101184>.
- [115] Rahim TNAT, Abdulla AM, Md Akil H. Recent developments in fused deposition modeling-based 3D printing of polymers and their composites. *Polym Rev* 2019;59(4):589–624. <http://dx.doi.org/10.1080/15583724.2019.1597883>.
- [116] Akhoundi B, Behravesh AH, Bagheri Saed A. Improving mechanical properties of continuous fiber-reinforced thermoplastic composites produced by FDM 3D printer. *J Reinf Plast Compos* 2019;38(3):99–116. <http://dx.doi.org/10.1177/0731684418807300>.

- [117] Sugiyama K, Matsuzaki R, Ueda M, Todoroki A, Hirano Y. 3D printing of composite sandwich structures using continuous carbon fiber and fiber tension. *Compos Part A Appl Sci Manuf* 2018;113:114–21. <http://dx.doi.org/10.1016/j.compositesa.2018.07.029>.
- [118] Shang J, Liu F, Zhang J, Chang B, Zhu C, Zhang W, Zhu Y, Ding X. Impact resistance of biomimetic gradient sinusoidal composites by 3D printing: Tunable structural stiffness and damage tolerance. *Compos Part B Eng* 2025;291:112016. <http://dx.doi.org/10.1016/j.compositesb.2024.112016>.
- [119] Chang T-C, Bechara Senior A, Celik H, Brands D, Yanev A, Osswald T. Validation of fiber breakage in simple shear flow with direct fiber simulation. *J Compos Sci* 2020;4(3):134. <http://dx.doi.org/10.3390/jcs4030134>.
- [120] Serdeczny MP, Comminal R, Mollah MT, Pedersen DB, Spangenberg J. Numerical modeling of the polymer flow through the hot-end in filament-based material extrusion additive manufacturing. *Addit Manuf* 2020;36:101454. <http://dx.doi.org/10.1016/j.addma.2020.101454>.
- [121] Kattinger J, Ebinger T, Kurz R, Bonten C. Numerical simulation of the complex flow during material extrusion in fused filament fabrication. *Addit Manuf* 2022;49:102476. <http://dx.doi.org/10.1016/j.addma.2021.102476>.
- [122] Ufodike CO, Nzebuka GC. Investigation of thermal evolution and fluid flow in the hot-end of a material extrusion 3D printer using melting model. *Addit Manuf* 2022;49:102502. <http://dx.doi.org/10.1016/j.addma.2021.102502>.
- [123] Phan DD, Horner JS, Swain ZR, Beris AN, Mackay ME. Computational fluid dynamics simulation of the melting process in the fused filament fabrication additive manufacturing technique. *Addit Manuf* 2020;33:101161. <http://dx.doi.org/10.1016/j.addma.2020.101161>.
- [124] Zhang J, Vasiliauskaite E, De Kuyper A, De Schryver C, Vogeler F, Desplenter F, Ferraris E. Temperature analyses in fused filament fabrication: from filament entering the hot-end to the printed parts. *3D Print Addit Manuf* 2022;9(2):132–42. <http://dx.doi.org/10.1089/3dp.2020.0339>.
- [125] Bellini A, Gu’ eri Su, Bertoldi M. Liquefier dynamics in fused deposition. *J Manuf Sci Eng* 2004;126(2):237–46. <http://dx.doi.org/10.1115/1.1688377>.
- [126] Osswald TA, Puentes J, Kattinger J. Fused filament fabrication melting model. *Addit Manuf* 2018;22:51–9. <http://dx.doi.org/10.1016/j.addma.2018.04.030>.
- [127] Go J, Schiffres SN, Stevens AG, Hart AJ. Rate limits of additive manufacturing by fused filament fabrication and guidelines for high-throughput system design. *Addit Manuf* 2017;16:1–11. <http://dx.doi.org/10.1016/j.addma.2017.03.007>.
- [128] Xu X, Ren H, Chen S, Luo X, Zhao F, Xiong Y. Review on melt flow simulations for thermoplastics and their fiber reinforced composites in fused deposition modeling. *J Manuf Process* 2023;92:272–86. <http://dx.doi.org/10.1016/j.jmapro.2023.02.039>.
- [129] Albrecht H, Savandaiah C, Lepschi A, Löw-Baselli B, Haider A. Parametric study in co-extrusion-based additive manufacturing of continuous fiber-reinforced plastic composites. In: Sim-AM 2019 II int. conf. simul. addit. manuf. CIMNE; 2019, p. 417–27.
- [130] Fu Y, Kan Y, Fan X, Xuan S, Yao X. Novel designable strategy and multi-scale analysis of 3D printed thermoplastic fabric composites. *Compos Sci Technol* 2022;222:109388. <http://dx.doi.org/10.1016/j.compscitech.2022.109388>.
- [131] Peng F, Vogt BD, Cakmak M. Complex flow and temperature history during melt extrusion in material extrusion additive manufacturing. *Addit Manuf* 2018;22:197–206. <http://dx.doi.org/10.1016/j.addma.2018.05.015>.
- [132] N. Turner B, Strong R, A. Gold S. A review of melt extrusion additive manufacturing processes: I. Process design and modeling. *Rapid Prototyp J* 2014;20(3):192–204. <http://dx.doi.org/10.1108/RPJ-01-2013-0012>.
- [133] Van Waeleghem T, Marchesini FH, Cardon L, D’hooge DR. Melt exit flow modelling and experimental validation for fused filament fabrication: From Newtonian to non-Newtonian effects. *J Manuf Process* 2022;77:138–50. <http://dx.doi.org/10.1016/j.jmapro.2022.03.002>.
- [134] Wang J, Ge X, Liu Y, Qi Z, Li L, Sun S, Yang Y. A review on theoretical modelling for shearing viscosities of continuous fibre-reinforced polymer composites. *Rheol Acta* 2019;58:321–31. <http://dx.doi.org/10.1007/s00397-019-01151-1>.
- [135] Wang J, Han Y, Ge X, Qi Z, Zhao J, Wang R, Wu H, Han T, Sun S, Wang H, et al. Fully predictive micro-mechanical modelling for shear viscosities of continuous fiber reinforced polymer composites. *Appl Compos Mater* 2023;30(4):1081–96. <http://dx.doi.org/10.1007/s10443-022-10083-8>.
- [136] Zhang H, Zhang L, Zhang H, Wu J, An X, Yang D. Fibre bridging and nozzle clogging in 3D printing of discontinuous carbon fibre-reinforced polymer composites: Coupled CFD-DEM modelling. *Int J Adv Manuf Technol* 2021;117(11–12):3549–62. <http://dx.doi.org/10.1007/s00170-021-07913-7>.
- [137] Wang Z, Smith DE, Jack DA. A statistical homogenization approach for incorporating fiber aspect ratio distribution in large area polymer composite deposition additive manufacturing property predictions. *Addit Manuf* 2021;43:102006. <http://dx.doi.org/10.1016/j.addma.2021.102006>.
- [138] Heller BP, Smith DE, Jack DA. Simulation of planar deposition polymer melt flow and fiber orientation in fused filament fabrication. In: 2017 int. solid freeform fabr. symp., University of Texas at Austin; 2017.
- [139] Han N, Cheng J, Yang J, Liu Y, Huang W. Design and implementation of 3D printing system for continuous CFRP composites. In: MATEC web conf. vol. 213, EDP Sciences; 2018, p. 01011. <http://dx.doi.org/10.1051/matecconf/201821301011>.
- [140] Markauskas D, Krugel-Emden H, Sivanesapillai R, Steeb H. Comparative study on mesh-based and mesh-less coupled CFD-DEM methods to model particle-laden flow. *Powder Technol* 2017;305:78–88. <http://dx.doi.org/10.1016/j.powtec.2016.09.052>.
- [141] Nasar A, Rogers BD, Revell A, Stansby P. Flexible slender body fluid interaction: Vector-based discrete element method with Eulerian smoothed particle hydrodynamics. *Comput & Fluids* 2019;179:563–78. <http://dx.doi.org/10.1016/j.compfluid.2018.11.024>.
- [142] Gröger B, Wang J, Bätzter T, Hornig A, Gude M. Modelling and simulation strategies for fluid-structure-interactions of highly viscous thermoplastic melt and single fibres—A numerical study. *Materials* 2022;15(20):7241. <http://dx.doi.org/10.3390/ma15207241>.
- [143] van Loon R, Anderson PD, van de Vosse FN, Sherwin SJ. Comparison of various fluid-structure interaction methods for deformable bodies. *Comput Struct* 2007;85(11–14):833–43. <http://dx.doi.org/10.1016/j.compstruc.2007.01.010>.
- [144] Chen L, Deng T, Zhou H, Huang Z, Peng X, Zhou H. A numerical simulation method for the one-step compression-stamping process of continuous fiber reinforced thermoplastic composites. *Polymers* 2021;13(19):3237. <http://dx.doi.org/10.3390/polym13193237>.
- [145] Sotiropoulos F, Yang X. Immersed boundary methods for simulating fluid-structure interaction. *Prog Aerosp Sci* 2014;65:1–21. <http://dx.doi.org/10.1016/j.paerosci.2013.09.003>.
- [146] Tornberg A-K, Shelley MJ. Simulating the dynamics and interactions of flexible fibers in Stokes flows. *J Comput Phys* 2004;196(1):8–40. <http://dx.doi.org/10.1016/j.jcp.2003.10.017>.
- [147] Kunhappan D, Harthong B, Chareyre B, Balarac G, Dumont PJ. Numerical modeling of high aspect ratio flexible fibers in inertial flows. *Phys Fluids* 2017;29(9). <http://dx.doi.org/10.1063/1.5001514>.
- [148] Bellehumeur C, Li L, Sun Q, Gu P. Modeling of bond formation between polymer filaments in the fused deposition modeling process. *J Manuf Process* 2004;6(2):170–8. [http://dx.doi.org/10.1016/S1526-6125\(04\)70071-7](http://dx.doi.org/10.1016/S1526-6125(04)70071-7).
- [149] Bähr F, Westkämper E. Correlations between influencing parameters and quality properties of components produced by fused deposition modeling. *Procedia CIRP* 2018;72:1214–9. <http://dx.doi.org/10.1016/j.procir.2018.03.048>.
- [150] Costa S, Duarte F, Covas J. Estimation of filament temperature and adhesion development in fused deposition techniques. *J Mater Process Technol* 2017;245:167–79. <http://dx.doi.org/10.1016/j.jmatprotect.2017.02.026>.
- [151] Costa S, Duarte F, Covas J. Thermal conditions affecting heat transfer in FDM/FFE: a contribution towards the numerical modelling of the process: This paper investigates convection, conduction and radiation phenomena in the filament deposition process. *Virtual Phys Prototyp* 2015;10(1):35–46. <http://dx.doi.org/10.1080/17452759.2014.984042>.
- [152] Brenken B, Favalo A, Barocio E, DeNardo NM, Pipes RB. Development of a model to predict temperature history and crystallization behavior of 3D printed parts made from fiber-reinforced thermoplastic polymers. In: Int. SAMPE tech. conf., vol. 12, 2016, p. 704.
- [153] Chen G, Wang D, Hua W, Wu W, Zhou W, Jin Y, Zheng W. Simulating and predicting the part warping in fused deposition modeling by thermal-structural coupling analysis. *3D Print Addit Manuf* 2023;10(1):70–82. <http://dx.doi.org/10.1089/3dp.2021.0119>.
- [154] El Moumen A, Tarfaoui M, Laifi K. Modelling of the temperature and residual stress fields during 3D printing of polymer composites. *Int J Adv Manuf Technol* 2019;104:1661–76. <http://dx.doi.org/10.1007/s00170-019-03965-y>.
- [155] Zhang J, Wang XZ, Yu WW, Deng YH. Numerical investigation of the influence of process conditions on the temperature variation in fused deposition modeling. *Mater Des* 2017;130:59–68. <http://dx.doi.org/10.1016/j.matdes.2017.05.040>.
- [156] Zhai S, Zhang P, Xian Y, Zeng J, Shi B. Effective thermal conductivity of polymer composites: Theoretical models and simulation models. *Int J Heat Mass Transfer* 2018;117:358–74. <http://dx.doi.org/10.1016/j.ijheatmasstransfer.2017.09.067>.
- [157] Ibrahim Y, Elkholly A, Schofield JS, Melenka GW, Kempers R. Effective thermal conductivity of 3D-printed continuous fiber polymer composites. *Adv Manuf Polym Compos Sci* 2020;6(1):17–28. <http://dx.doi.org/10.1080/20550340.2019.1710023>.
- [158] Islam S, Bhat G. A model for predicting thermal conductivity of porous composite materials. *Heat Mass Transf* 2023;59(11):2023–34. <http://dx.doi.org/10.1007/s00231-023-03380-w>.
- [159] Chen H, Ginzburg VV, Yang J, Yang Y, Liu W, Huang Y, Du L, Chen B. Thermal conductivity of polymer-based composites: Fundamentals and applications. *Prog Polym Sci* 2016;59:41–85. <http://dx.doi.org/10.1016/j.progpolymsci.2016.03.001>.
- [160] Xiao J, Xu Y, Zhang F. An analytical method for predicting the effective transverse thermal conductivity of nano coated fiber composites. *Compos Struct* 2018;189:553–9. <http://dx.doi.org/10.1016/j.compstruct.2018.01.086>.
- [161] min Kim H, Lee S, Song YS, Lee D. Synergistic improvement of electrical and thermal conductivities of carbon-based nanocomposites and its prediction by Mori-Tanaka scheme with interfacial resistances. *Compos Struct* 2019;211:56–62. <http://dx.doi.org/10.1016/j.compstruct.2018.12.018>.

- [162] Gayton JT, Lapp JL. Evaluation of theoretical models for anisotropic effective thermal conductivity in continuous fiber-reinforced thermoplastic laminates. *Internat J Numer Methods Heat Fluid Flow* 2025;35(1):168–98. <http://dx.doi.org/10.1108/HFF-05-2024-0340>.
- [163] Kiradjiev KB, Halvorsen SA, Van Gorder RA, Howison SD. Maxwell-type models for the effective thermal conductivity of a porous material with radiative transfer in the voids. *Int J Therm Sci* 2019;145:106009. <http://dx.doi.org/10.1016/j.ijthermalsci.2019.106009>.
- [164] Wang G, Huang Y, Gao M, Chen Q. Micromechanics of thermal conductive composites: review, developments and applications. *Acta Mech Solida Sin* 2024;37(2):215–37. <http://dx.doi.org/10.1007/s10338-024-00469-5>.
- [165] Comminal R, Serdeczny MP, Pedersen DB, Spangenberg J. Numerical modeling of the strand deposition flow in extrusion-based additive manufacturing. *Addit Manuf* 2018;20:68–76. <http://dx.doi.org/10.1016/j.addma.2017.12.013>.
- [166] Xia H, Lu J, Tryggvason G. A numerical study of the effect of viscoelastic stresses in fused filament fabrication. *Comput Methods Appl Mech Engrg* 2019;346:242–59. <http://dx.doi.org/10.1016/j.cma.2018.11.031>.
- [167] Xia H, Lu J, Dabiri S, Tryggvason G. Fully resolved numerical simulations of fused deposition modeling. Part I: fluid flow. *Rapid Prototyp J* 2018;24(2):463–76. <http://dx.doi.org/10.1108/RPJ-12-2016-0217>.
- [168] Jahandaroost M, Milani AS. Multiphysics modeling and experimental investigation of the deposition process in fused filament fabrication method, under high-viscosity and non-newtonian material flow. *J Mater Eng Perform* 2021;30(9):6913–23. <http://dx.doi.org/10.1007/s11665-021-06061-z>.
- [169] Comminal R, Spangenberg J, Hattel JH. Cellwise conservative unsplit advection for the volume of fluid method. *J Comput Phys* 2015;283:582–608. <http://dx.doi.org/10.1016/j.jcp.2014.12.003>.
- [170] Comminal R, Serdeczny MP, Pedersen DB, Spangenberg J. Motion planning and numerical simulation of material deposition at corners in extrusion additive manufacturing. *Addit Manuf* 2019;29:100753. <http://dx.doi.org/10.1016/j.addma.2019.06.005>.
- [171] McIlroy C, Olmsted P. Disentanglement effects on welding behaviour of polymer melts during the fused-filament-fabrication method for additive manufacturing. *Polymer* 2017;123:376–91. <http://dx.doi.org/10.1016/j.polymer.2017.06.051>.
- [172] Sun Q, Rizvi G, Bellehumeur C, Gu P. Effect of processing conditions on the bonding quality of FDM polymer filaments. *Rapid Prototyp J* 2008;14(2):72–80. <http://dx.doi.org/10.1108/13552540810862028>.
- [173] Vaes D, Van Puyvelde P. Semi-crystalline feedstock for filament-based 3D printing of polymers. *Prog Polym Sci* 2021;118:101411. <http://dx.doi.org/10.1016/j.progpolymsci.2021.101411>.
- [174] Zhang M, Tian X, Li D. Interfacial transcrystallization and mechanical performance of 3D-printed fully recyclable continuous fiber self-reinforced composites. *Polymers* 2021;13(18):3176. <http://dx.doi.org/10.3390/polym13183176>.
- [175] Gurrala PK, Regalla SP. Part strength evolution with bonding between filaments in fused deposition modelling: This paper studies how coalescence of filaments contributes to the strength of final FDM part. *Virtual Phys Prototyp* 2014;9(3):141–9. <http://dx.doi.org/10.1080/17452759.2014.913400>.
- [176] Brenken Bar, Barocio E, Favoloro A, Kunc V, Pipes RB. Fused filament fabrication of fiber-reinforced polymers: a review. *Addit Manuf* 2018;21:1–16. <http://dx.doi.org/10.1016/j.addma.2018.01.002>.
- [177] Lee WI, Talbott MF, Springer GS, Berglund LA. Effects of cooling rate on the crystallinity and mechanical properties of thermoplastic composites. *J Reinf Plast Compos* 1987;6(1):2–12. <http://dx.doi.org/10.1177/073168448700600101>.
- [178] Pu J, McIlroy C, Jones A, Ashcroft I. Understanding mechanical properties in fused filament fabrication of polyether ether ketone. *Addit Manuf* 2021;37:101673. <http://dx.doi.org/10.1016/j.addma.2020.101673>.
- [179] Yang D, Cao Y, Zhang Z, Yin Y, Li D. Effects of crystallinity control on mechanical properties of 3D-printed short-carbon-fiber-reinforced polyether ether ketone composites. *Polym Test* 2021;97:107149. <http://dx.doi.org/10.1016/j.polymertesting.2021.107149>.
- [180] Avrami M. Kinetics of phase change. I general theory. *J Chem Phys* 1939;7(12):1103–12. <http://dx.doi.org/10.1063/1.1750380>.
- [181] Samy AA, Golbang A, Harkin-Jones E, Archer E, McIlhagger A. Prediction of part distortion in fused deposition modelling (FDM) of semi-crystalline polymers via COMSOL: Effect of printing conditions. *CIRP J Manuf Sci Technol* 2021;33:443–53. <http://dx.doi.org/10.1016/j.cirpj.2021.04.012>.
- [182] Lu X, Detrez F, Roland S. Numerical study of the relationship between the spherulitic microstructure and isothermal crystallization kinetics. Part I. 2-D analyses. *Polymer* 2019;179:121642. <http://dx.doi.org/10.1016/j.polymer.2019.121642>.
- [183] Gao X, Qi S, Yang B, Su Y, Li J, Wang D. Synergistic effect of plasticizer and nucleating agent on crystallization behavior of polylactide during fused filament fabrication. *Polymer* 2021;215:123426. <http://dx.doi.org/10.1016/j.polymer.2021.123426>.
- [184] Zhang T, Xu Y, Li H, Zhang B. Interfacial adhesion between carbon fibers and nylon 6: Effect of fiber surface chemistry and grafting of nano-SiO<sub>2</sub>. *Compos Part A Appl Sci Manuf* 2019;121:157–68. <http://dx.doi.org/10.1016/j.compositesa.2019.03.029>.
- [185] Bin Y, Wang H. Transcristallization in polymer composites and nanocomposites. In: Cryst. multiphase polym. syst.. Elsevier; 2018, p. 341–65. <http://dx.doi.org/10.1016/B978-0-12-809453-2.00012-8>.
- [186] Li H, Xu Y, Zhang T, Niu K, Wang Y, Zhao Y, Zhang B. Interfacial adhesion and shear behaviors of aramid fiber/polyamide 6 composites under different thermal treatments. *Polym Test* 2020;81:106209. <http://dx.doi.org/10.1016/j.polymertesting.2019.106209>.
- [187] Ma X-l, Wen L-h, Wang S-y, Xiao J-y, Li W-h, Hou X. Inherent relationship between process parameters, crystallization and mechanical properties of continuous carbon fiber reinforced PEEK composites. *Def Technol* 2023;24:269–84. <http://dx.doi.org/10.1016/j.dt.2022.04.010>.
- [188] Pisani WA, Radue MS, Chinkanjanarot S, Bednarczyk BA, Pineda EJ, Waters K, Pandey R, King JA, Odegard GM. Multiscale modeling of PEEK using reactive molecular dynamics modeling and micromechanics. *Polymer* 2019;163:96–105. <http://dx.doi.org/10.1016/j.polymer.2018.12.052>.
- [189] Park S, Moon J, Kim B, Cho M. Multi-scale coarse-grained molecular dynamics simulation to investigate the thermo-mechanical behavior of shape-memory polyurethane copolymers. *Polymer* 2021;213:123228. <http://dx.doi.org/10.1016/j.polymer.2020.123228>.
- [190] Ruan C, Ouyang J, Liu S. Multi-scale modeling and simulation of crystallization during cooling in short fiber reinforced composites. *Int J Heat Mass Transfer* 2012;55(7–8):1911–21. <http://dx.doi.org/10.1016/j.ijheatmasstransfer.2011.11.046>.
- [191] Durin A, Chenot J-L, Haudin J-M, Boyard N, Bailleul J-L. Simulating polymer crystallization in thin films: Numerical and analytical methods. *Eur Polym J* 2015;73:1–16. <http://dx.doi.org/10.1016/j.eurpolymj.2015.10.001>.
- [192] Wang X, Ouyang J, Zhou W, Liu Z. A phase field technique for modeling and predicting flow induced crystallization morphology of semi-crystalline polymers. *Polymers* 2016;8(6):230. <http://dx.doi.org/10.3390/polym8060230>.
- [193] Gránásy L, Rátkai L, Szálás A, Korbuly B, Tóth GI, Környei L, Puszta T. Phase-field modeling of polycrystalline solidification: from needle crystals to spherulites—a review. *Metall Mater Trans A* 2014;45:1694–719. <http://dx.doi.org/10.1007/s11661-013-1988-0>.
- [194] Liu Z, Zhou Z, Ming Y, Zhang S, Hao T, Nie Y. Molecular dynamics simulations of nucleation details in stretched polyethylene. *Polymer* 2020;195:122442. <http://dx.doi.org/10.1016/j.polymer.2020.122442>.
- [195] Wang J, in't Veld PJ, Robbins MO, Ge T. Effects of coarse-graining on molecular simulation of craze formation in polymer glass. *Macromolecules* 2022;55(4):1267–78. <http://dx.doi.org/10.1021/acs.macromol.1c01969>.
- [196] Darbaniyan F, Yan X, Sharma P. An atomistic perspective on the effect of strain rate and lithium fraction on the mechanical behavior of silicon electrodes. *J Appl Mech* 2020;87(3):031011. <http://dx.doi.org/10.1115/1.4045545>.
- [197] Yan X, Sharma P. Time-scaling in atomistics and the rate-dependent mechanical behavior of nanostructures. *Nano Lett* 2016;16(6):3487–92. <http://dx.doi.org/10.1021/acs.nanolett.6b00117>.
- [198] Yan X, Cao P, Tao W, Sharma P, Park HS. Atomistic modeling at experimental strain rates and timescales. *J Phys D* 2016;49(49):493002. <http://dx.doi.org/10.1088/0022-3727/49/49/493002>.
- [199] Yu N, Sun X, Wang Z, Zhang D, Li J. Effects of auxiliary heat on warpage and mechanical properties in carbon fiber/ABS composite manufactured by fused deposition modeling. *Mater Des* 2020;195:108978. <http://dx.doi.org/10.1016/j.matedes.2020.108978>.
- [200] Chinesta F, Ammar A, Cueto E. Recent advances and new challenges in the use of the proper generalized decomposition for solving multidimensional models. *Arch Comput Methods Eng* 2010;17(4):327–50. <http://dx.doi.org/10.1007/s11831-010-9049-y>.
- [201] Tian X, Liu T, Wang Q, Dilmurat A, Li D, Ziegmann G. Recycling and remanufacturing of 3D printed continuous carbon fiber reinforced PLA composites. *J Clean Prod* 2017;142:1609–18. <http://dx.doi.org/10.1016/j.jclepro.2016.11.139>.
- [202] An Y, Myung JH, Yoon J, Yu W-R. Three-dimensional printing of continuous carbon fiber-reinforced polymer composites via in-situ pin-assisted melt impregnation. *Addit Manuf* 2022;55:102860. <http://dx.doi.org/10.1016/j.addma.2022.102860>.
- [203] Arrigo R, Frache A. FDM printability of PLA based-materials: the key role of the rheological behavior. *Polymers* 2022;14(9):1754. <http://dx.doi.org/10.3390/polym14091754>.
- [204] Calafel I, Aguirresarobe R, Peñas M, Santamaría A, Tierro M, Conde J, Pascual B. Searching for rheological conditions for FFF 3D printing with PVC based flexible compounds. *Materials* 2020;13(1):178. <http://dx.doi.org/10.3390/ma13010178>.
- [205] Kobayashi S, Tsukada T, Morimoto T. Resin impregnation behavior in carbon fiber reinforced polyamide 6 composite: Effects of yarn thickness, fabric lamination and sizing agent. *Compos Part A Appl Sci Manuf* 2017;101:283–9. <http://dx.doi.org/10.1016/j.compositesa.2017.06.030>.
- [206] Ding X, He Q, Yang Q, Wang S, Chen K. Numerical simulation of impregnation process of reactive injection pultrusion for glass fiber/PA6 composites. *Polymers* 2022;14(4):666. <http://dx.doi.org/10.3390/polym14040666>.
- [207] Gebart BR. Permeability of unidirectional reinforcements for RTM. *J Compos Mater* 1992;26(8):1100–33. <http://dx.doi.org/10.1177/002199839202600802>.

- [208] Bodaghi M, Lomov S, Simacek P, Correia N, Advani S. On the variability of permeability induced by reinforcement distortions and dual scale flow in liquid composite moulding: A review. *Compos Part A Appl Sci Manuf* 2019;120:188–210. <http://dx.doi.org/10.1016/j.compositesa.2019.03.004>.
- [209] Yazdchi K, Srivastava S, Luding S. Micro-macro relations for flow through random arrays of cylinders. *Compos Part A Appl Sci Manuf* 2012;43(11):2007–20. <http://dx.doi.org/10.1016/j.compositesa.2012.07.020>.
- [210] Gommer F, Endruweit A, Long AC. Analysis of filament arrangements and generation of statistically equivalent composite micro-structures. *Compos Sci Technol* 2014;99:45–51. <http://dx.doi.org/10.1016/j.compscitech.2014.05.008>.
- [211] Endruweit A, Gommer F, Long A. Stochastic analysis of fibre volume fraction and permeability in fibre bundles with random filament arrangement. *Compos Part A Appl Sci Manuf* 2013;49:109–18. <http://dx.doi.org/10.1016/j.compositesa.2013.02.012>.
- [212] Vernet N, Ruiz E, Advani S, Alms JB, Aubert M, Barburski M, Barari B, Beraud JM, Berg DC, Correia N, et al. Experimental determination of the permeability of engineering textiles: Benchmark II. *Compos Part A Appl Sci Manuf* 2014;61:172–84. <http://dx.doi.org/10.1016/j.compositesa.2014.02.010>.
- [213] Schell J, Siegrist M, Ermanni P. Experimental determination of the transversal and longitudinal fibre bundle permeability. *Appl Compos Mater* 2007;14(2):117–28. <http://dx.doi.org/10.1007/s10443-007-9035-1>.
- [214] Merhi D, Michaud V, Kämpfer L, Vuillomenet P, Månsen JA. Transverse permeability of chopped fibre bundle beds. *Compos Part A Appl Sci Manuf* 2007;38(3):739–46. <http://dx.doi.org/10.1016/j.compositesa.2006.09.006>.
- [215] Ngo SI, Lim Y-I, Hahn M-H, Jung J. Prediction of degree of impregnation in thermoplastic unidirectional carbon fiber prepreg by multi-scale computational fluid dynamics. *Chem Eng Sci* 2018;185:64–75. <http://dx.doi.org/10.1016/j.ces.2018.04.010>.
- [216] Wang K, Huang Y, Cheng P, Xiong Y, Le Dugou A, Peng Y, Rao Y, Ahzi S. Novel application of dual-nozzle 3D printer for enhanced in-situ impregnation 3D printing of dry continuous fiber reinforced composites. *Compos Part A Appl Sci Manuf* 2024;183:108231. <http://dx.doi.org/10.1016/j.compositesa.2024.108231>.
- [217] Hou Z, Tian X, Zhang J, Zheng Z, Zhe L, Li D, Malakhov AV, Polilov AN. Optimization design and 3D printing of curvilinear fiber reinforced variable stiffness composites. *Compos Sci Technol* 2021;201:108502. <http://dx.doi.org/10.1016/j.compscitech.2020.108502>.
- [218] Malakhov AV, Tian X, Zheng Z, Plugat TP, Huang Y, Tatus NA, Li D. Three-dimensional printing of biomimetic variable stiffness composites with controlled orientations and volume fraction of fibers. *Compos Struct* 2022;299:116091. <http://dx.doi.org/10.1016/j.compstruct.2022.116091>.
- [219] Chen Y, Ye L. Topological design for 3D-printing of carbon fibre reinforced composite structural parts. *Compos Sci Technol* 2021;204:108644. <http://dx.doi.org/10.1016/j.compscitech.2020.108644>.
- [220] Yang Z, Fu K, Zhang Z, Zhang J, Li Y. Topology optimization of 3D-printed continuous fiber-reinforced composites considering manufacturability. *Compos Sci Technol* 2022;230:109727. <http://dx.doi.org/10.1016/j.compscitech.2022.109727>.
- [221] Huang Y, Tian X, Zheng Z, Li D, Malakhov AV, Polilov AN. Multiscale concurrent design and 3D printing of continuous fiber reinforced thermoplastic composites with optimized fiber trajectory and topological structure. *Compos Struct* 2022;285:115241. <http://dx.doi.org/10.1016/j.compstruct.2022.115241>.
- [222] Wei G, Chen Y, Li Q, Fu K. Multiscale topology optimisation for porous composite structures with stress-constraint and clustered microstructures. *Comput Methods Appl Mech Engng* 2023;416:116329. <http://dx.doi.org/10.1016/j.cma.2023.116329>.
- [223] Li G, Chen Y, Li Q. Strength-based collaborative topology optimization for continuous fiber reinforced composites. *Comput Methods Appl Mech Engng* 2024;430:117206. <http://dx.doi.org/10.1016/j.cma.2024.117206>.
- [224] Li G, Chen Y. Highly efficient and extensible parallel topology optimization for continuous fiber reinforced composites. *Comput Methods Appl Mech Engng* 2025;436:117713. <http://dx.doi.org/10.1016/j.cma.2024.117713>.
- [225] Avanzini A, Battini D, Giorleo L. Finite element modelling of 3D printed continuous carbon fiber composites: Embedded elements technique and experimental validation. *Compos Struct* 2022;292:115631. <http://dx.doi.org/10.1016/j.compstruct.2022.115631>.
- [226] Qian P, Xu Q, et al. Development of embedded element technique for permeability analysis of cracked porous media. *Math Probl Eng* 2017;2017. <http://dx.doi.org/10.1155/2017/6713452>.
- [227] de Kergariou C, Kim BC, Perriman A, Le Dugou A, Guessasma S, Scarpa F. Design of 3D and 4D printed continuous fibre composites via an evolutionary algorithm and voxel-based finite elements: Application to natural fibre hygroscopic. *Addit Manuf* 2022;59:103144. <http://dx.doi.org/10.1016/j.addma.2022.103144>.
- [228] Jiang B, Zhang M, Fu L, Zhou M, Zhai Z. Molecular dynamics simulation on the interfacial behavior of over-molded hybrid fiber reinforced thermoplastic composites. *Polymers* 2020;12(6):1270. <http://dx.doi.org/10.3390/polym12061270>.
- [229] Han C, Lyu D, Lu Y, Men Y. Crystallinity and temperature dependent mechanical properties of poly (4-methyl-1-pentene). *Polymer* 2023;269:125734. <http://dx.doi.org/10.1016/j.polymer.2023.125734>.
- [230] Horn TD, Heidrich D, Wulf H, Gehde M, Ihlemann J. Multiscale simulation of semi-crystalline polymers to predict mechanical properties. *Polymers* 2021;13(19):3233. <http://dx.doi.org/10.3390/polym13193233>.
- [231] Talreja R. A mechanisms-based framework for describing failure in composite materials. In: Beaumont P, Soutis C, Hodzic A, editors. *Structural integrity and durability of advanced composites*. Woodhead publishing series in composites science and engineering, Woodhead Publishing; 2015, p. 25–42. <http://dx.doi.org/10.1016/B978-0-08-100137-0-00002-X>.
- [232] Talreja R. Assessment of the fundamentals of failure theories for composite materials. *Compos Sci Technol* 2014;105:190–201. <http://dx.doi.org/10.1016/j.compscitech.2014.10.014>.
- [233] Fu Y, Yao X. A review on manufacturing defects and their detection of fiber reinforced resin matrix composites. *Compos Part C Open Access* 2022;8:100276. <http://dx.doi.org/10.1016/j.jcomc.2022.100276>.
- [234] Hoshikawa Y, Shirasu K, Yamamoto K, Hirata Y, Higuchi R, Okabe T. Open-hole tensile properties of 3D-printed continuous carbon-fiber-reinforced thermoplastic laminates: experimental study and multiscale analysis. *J Thermoplast Compos Mater* 2023;36(7):2836–61. <http://dx.doi.org/10.1177/0897057221110791>.
- [235] Tang H, Sun Q, Li Z, Su X, Yan W. Longitudinal compression failure of 3D printed continuous carbon fiber reinforced composites: An experimental and computational study. *Compos Part A Appl Sci Manuf* 2021;146:106416. <http://dx.doi.org/10.1016/j.compositesa.2021.106416>.
- [236] Zhang K, Zhang H, Wu J, Chen J, Yang D. Improved fibre placement in filament-based 3D printing of continuous carbon fibre reinforced thermoplastic composites. *Compos Part A Appl Sci Manuf* 2023;168:107454. <http://dx.doi.org/10.1016/j.compositesa.2023.107454>.
- [237] Hoshikawa Y, Shirasu K, Higuchi R, Kawagoe Y, Tohmyoh H, Okabe T. Experimental and numerical investigation of the relationship between material defects and elastoplastic behavior of 3D-printed carbon-fiber-reinforced thermoplastics under compressive loading. *Compos Sci Technol* 2023;241:110116. <http://dx.doi.org/10.1016/j.compscitech.2023.110116>.
- [238] Sebaey T, Catalanotti G, O'Dowd N. A microscale integrated approach to measure and model fibre misalignment in fibre-reinforced composites. *Compos Sci Technol* 2019;183:107793. <http://dx.doi.org/10.1016/j.compscitech.2019.107793>.
- [239] Dutra TA, Ferreira RTL, Resende HB, Blinzler BJ, Asp LE. Mechanism based failure of 3D-printed continuous carbon fiber reinforced thermoplastic composites. *Compos Sci Technol* 2021;213:108962. <http://dx.doi.org/10.1016/j.compscitech.2021.108962>.
- [240] Zhang X, Zheng X, Han Y, Tian Y, Zhang D, Yan L. Failure mechanisms and process defects of 3D-printed continuous carbon fiber-reinforced composite circular honeycomb structures with different stacking directions. *Aerospace Sci Technol* 2020;148:109075. <http://dx.doi.org/10.1016/j.ast.2020.109075>.
- [241] Tekinalp HL, Kunc V, Velez-Garcia GM, Duty CE, Love LJ, Naskar AK, Blue CA, Ozcan S. Highly oriented carbon fiber-polymer composites via additive manufacturing. *Compos Sci Technol* 2014;105:144–50. <http://dx.doi.org/10.1016/j.compscitech.2014.10.009>.
- [242] Liebig WV, Viets C, Schulte K, Fiedler B. Influence of voids on the compressive failure behaviour of fibre-reinforced composites. *Compos Sci Technol* 2015;117:225–33. <http://dx.doi.org/10.1016/j.compscitech.2015.06.020>.
- [243] Justo J, Távara L, García-Guzmán L, París F. Characterization of 3D printed long fibre reinforced composites. *Compos Struct* 2018;185:537–48. <http://dx.doi.org/10.1016/j.compstruct.2017.11.052>.
- [244] Polyzos E, Katalagarianakis A, Polyzos D, Van Hemelrijck D, Pyl L. A multiscale analytical methodology for the prediction of mechanical properties of 3D-printed materials with continuous fibres. *Addit Manuf* 2020;36:101394. <http://dx.doi.org/10.1016/j.addma.2020.101394>.
- [245] Melenka GW, Cheung BK, Schofield JS, Dawson MR, Carey JP. Evaluation and prediction of the tensile properties of continuous fiber-reinforced 3D printed structures. *Compos Struct* 2016;153:866–75. <http://dx.doi.org/10.1016/j.compstruct.2016.07.018>.
- [246] Polyzos E, Van Hemelrijck D, Pyl L. Numerical modelling of the elastic properties of 3D-printed specimens of thermoplastic matrix reinforced with continuous fibres. *Compos Part B Eng* 2021;211:108671. <http://dx.doi.org/10.1016/j.compositesb.2021.108671>.
- [247] van de Werken N, Hurley J, Khanboluki P, Sarvestani AN, Tamjani AY, Tehrani M. Design considerations and modeling of fiber reinforced 3D printed parts. *Compos Part B Eng* 2019;160:684–92. <http://dx.doi.org/10.1016/j.compositesb.2018.12.094>.
- [248] Caminero M, Chacón J, García-Moreno I, Reverte J. Interlaminar bonding performance of 3D printed continuous fibre reinforced thermoplastic composites using fused deposition modelling. *Polym Test* 2018;68:415–23. <http://dx.doi.org/10.1016/j.polymertesting.2018.04.038>.
- [249] Pan F, Jiang X, Sun S, Wang M, Cao W. Design and construction for the interface between carbon fiber and epoxy via vinyl alkoxysilane modification. *Compos Part A Appl Sci Manuf* 2022;162:107148. <http://dx.doi.org/10.1016/j.compositesa.2022.107148>.

- [250] Wang R, Han J, Mao J, Hu D, Liu X, Guo X. A molecular dynamics based cohesive zone model for interface failure under monotonic tension of 3D four direction SiCf/SiC composites. *Compos Struct* 2021;274:114397. <http://dx.doi.org/10.1016/j.compstruct.2021.114397>.
- [251] Shen W, Zhou T, Shi X. Enhanced sampling in molecular dynamics simulations and their latest applications—A review. *Nano Res* 2023;16(12):13474–97. <http://dx.doi.org/10.1007/s12274-023-6311-9>.
- [252] Joshi SY, Deshmukh SA. A review of advancements in coarse-grained molecular dynamics simulations. *Mol Simul* 2021;47(10–11):786–803. <http://dx.doi.org/10.1080/08927022.2020.1828583>.
- [253] Polyzos E, Katalagarianakis A, Van Hemelrijck D, Pyl L. Delamination analysis of 3D-printed nylon reinforced with continuous carbon fibers. *Addit Manuf* 2021;46:102144. <http://dx.doi.org/10.1016/j.addma.2021.102144>.
- [254] Yavas D, Zhang Z, Liu Q, Wu D. Fracture behavior of 3D printed carbon fiber-reinforced polymer composites. *Compos Sci Technol* 2021;208:108741. <http://dx.doi.org/10.1016/j.compscitech.2021.108741>.
- [255] Mehdikhani M, Gorbatikh L, Verpoest I, Lomov SV. Voids in fiber-reinforced polymer composites: A review on their formation, characteristics, and effects on mechanical performance. *J Compos Mater* 2019;53(12):1579–669. <http://dx.doi.org/10.1177/0021998318772152>.
- [256] Talreja R. *Failure analysis of composite materials with manufacturing defects*. CRC Press; 2024.
- [257] Orifici AC, Herszberg I, Thomson RS. Review of methodologies for composite material modelling incorporating failure. *Compos Struct* 2008;86(1–3):194–210. <http://dx.doi.org/10.1016/j.compstruct.2008.03.007>.
- [258] Zimmermann N, Wang PH. A review of failure modes and fracture analysis of aircraft composite materials. *Eng Fail Anal* 2020;115:104692. <http://dx.doi.org/10.1016/j.engfailanal.2020.104692>.
- [259] Wan L, Ismail Y, Sheng Y, Ye J, Yang D. A review on micromechanical modelling of progressive failure in unidirectional fibre-reinforced composites. *Compos Part C Open Access* 2023;10:100348. <http://dx.doi.org/10.1016/j.jcomc.2023.100348>.
- [260] Liu P, Zheng J. Recent developments on damage modeling and finite element analysis for composite laminates: A review. *Mater Des* 2010;31(8):3825–34. <http://dx.doi.org/10.1016/j.matdes.2010.03.031>.
- [261] Zhu W, Fu L, Tian X, Zhi Q, Hou Z, Zhang Z, Wang N, Liu T, Sun H, Matsuzaki R, et al. Three-dimensional printing of high-performance continuous fiber-reinforced thermoplastic composites: causes and elimination of process-induced defects. *Compos Part B Eng* 2024;112080. <http://dx.doi.org/10.1016/j.compositesb.2024.112080>.
- [262] Pappas JM, Thakur AR, Leu MC, Dong X. A parametric study and characterization of additively manufactured continuous carbon fiber reinforced composites for high-speed 3D printing. *Int J Adv Manuf Technol* 2021;113:2137–51. <http://dx.doi.org/10.1007/s00170-021-06723-1>.
- [263] Li N, Link G, Jelonnek J, Morais MV, Henning F. Microwave additive manufacturing of continuous carbon fibers reinforced thermoplastic composites: Characterization, analysis, and properties. *Addit Manuf* 2021;44:102035. <http://dx.doi.org/10.1016/j.addma.2021.102035>.
- [264] Sadaghiani H, Dadmand B, Pourbaba M, Jabbari S, Yeon JH. The effect of size on the mechanical properties of 3D-printed polymers. *Sustainability* 2023;16(1):356. <http://dx.doi.org/10.3390/su16010356>.
- [265] Ye W, Dou H, Cheng Y, Zhang D, Lin S. Mechanical and self-sensing properties of 3D printed continuous carbon fiber reinforced composites. *Polym Compos* 2022;43(10):7428–37. <http://dx.doi.org/10.1002/pc.26825>.
- [266] Yao X, Luan C, Zhang D, Lan L, Fu J. Evaluation of carbon fiber-embedded 3D printed structures for strengthening and structural-health monitoring. *Mater Des* 2017;114:424–32. <http://dx.doi.org/10.1016/j.matdes.2016.10.078>.
- [267] Liu H, Zhang H, Han W, Lin H, Li R, Zhu J, Huang W. 3D printed flexible strain sensors: From printing to devices and signals. *Adv Mater* 2021;33(8):2004782. <http://dx.doi.org/10.1002/adma.202004782>.
- [268] Xu Y, Yang J, Bai X, Huang Q, Damil N, Hu H. Material database construction for data-driven computing via a continuous path-following method. *Compos Struct* 2023;319:117187. <http://dx.doi.org/10.1016/j.compstruct.2023.117187>.
- [269] Yang J, Li P, Zhang Y, Hui Y, Xu L, Damil N, Hu H. Unified functional based data-model-coupling computing for composite materials and structures. *Compos Struct* 2023;312:116840. <http://dx.doi.org/10.1016/j.compstruct.2023.116840>.
- [270] Wang C, Tan X, Tor S, Lim C. Machine learning in additive manufacturing: State-of-the-art and perspectives. *Addit Manuf* 2020;36:101538. <http://dx.doi.org/10.1016/j.addma.2020.101538>.
- [271] Cai R, Wang K, Wen W, Peng Y, Baniassadi M, Ahzi S. Application of machine learning methods on dynamic strength analysis for additive manufactured polypropylene-based composites. *Polym Test* 2022;110:107580. <http://dx.doi.org/10.1016/j.polymertesting.2022.107580>.
- [272] Cai R, Wen W, Wang K, Peng Y, Ahzi S, Chinesta F. Tailoring interfacial properties of 3D-printed continuous natural fiber reinforced polypropylene composites through parameter optimization using machine learning methods. *Mater Today Commun* 2022;32:103985. <http://dx.doi.org/10.1016/j.mtcomm.2022.103985>.
- [273] Fontes A, Shadmehri F. Data-driven failure prediction of fiber-reinforced polymer composite materials. *Eng Appl Artif Intell* 2023;120:105834. <http://dx.doi.org/10.1016/j.engappai.2023.105834>.
- [274] Stamopoulos A, Tserpes K, Dentsoras A. Quality assessment of porous CFRP specimens using X-ray computed tomography data and artificial neural networks. *Compos Struct* 2018;192:327–35. <http://dx.doi.org/10.1016/j.compstruct.2018.02.096>.
- [275] Tang Y, Wang Q, Cheng L, Li J, Ke Y. An in-process inspection method integrating deep learning and classical algorithm for automated fiber placement. *Compos Struct* 2022;300:116051. <http://dx.doi.org/10.1016/j.compstruct.2022.116051>.
- [276] Xu X, Wang G, Yan H, Zhang L, Yao X. Deep-learning-enhanced digital twinning of complex composite structures and real-time mechanical interaction. *Compos Sci Technol* 2023;241:110139. <http://dx.doi.org/10.1016/j.compscitech.2023.110139>.
- [277] Mukherjee T, DebRoy T. A digital twin for rapid qualification of 3D printed metallic components. *Appl Mater Today* 2019;14:59–65. <http://dx.doi.org/10.1016/j.apmt.2018.11.003>.
- [278] Ding S, Zou B, Liu Q, Wang X, Liu J, Li L. Non-planar additive manufacturing of pre-impregnated continuous fiber reinforced composites using a three-axis printer. *J Mater Res Technol* 2024;32:4410–9. <http://dx.doi.org/10.1016/j.jmrt.2024.09.032>.
- [279] Zhang K, Zhang W, Ding X. Multi-axis additive manufacturing process for continuous fibre reinforced composite parts. *Procedia CIRP* 2019;85:114–20. <http://dx.doi.org/10.1016/j.procir.2019.09.022>.
- [280] Liu S, Li Y, Li N. A novel free-hanging 3D printing method for continuous carbon fiber reinforced thermoplastic lattice truss core structures. *Mater Des* 2018;137:235–44. <http://dx.doi.org/10.1016/j.matdes.2017.10.007>.
- [281] Wang Z, Luan C, Liao G, Yao X, Fu J. Mechanical and self-monitoring behaviors of 3D printing smart continuous carbon fiber-thermoplastic lattice truss sandwich structure. *Compos Part B Eng* 2019;176:107215. <http://dx.doi.org/10.1016/j.compositesb.2019.107215>.
- [282] Eichenhofer M, Wong JC, Ermanni P. Continuous lattice fabrication of ultra-lightweight composite structures. *Addit Manuf* 2017;18:48–57. <http://dx.doi.org/10.1016/j.addma.2017.08.013>.
- [283] Shang J, Zhang W, Liu F, Wang S, Tian M, Ding X. Z-direction performance and failure behavior of 3D printed continuous fiber reinforced composites with sinusoidal structure. *Compos Sci Technol* 2023;239:110069. <http://dx.doi.org/10.1016/j.compscitech.2023.110069>.
- [284] Zeng C, Liu L, Bian W, Leng J, Liu Y. Temperature-dependent mechanical response of 4D printed composite lattice structures reinforced by continuous fiber. *Compos Struct* 2022;280:114952. <http://dx.doi.org/10.1016/j.compstruct.2021.114952>.
- [285] Le Duigou A, Fruleux T, Matsuzaki R, Chabaud G, Ueda M, Castro M. 4D printing of continuous flax-fibre based shape-changing hygromorph biocomposites: Towards sustainable metamaterials. *Mater Des* 2021;211:110158. <http://dx.doi.org/10.1016/j.matdes.2021.110158>.
- [286] Dong K, Ke H, Panahi-Sarmad M, Yang T, Huang X, Xiao X. Mechanical properties and shape memory effect of 4D printed cellular structure composite with a novel continuous fiber-reinforced printing path. *Mater Des* 2021;198:109303. <http://dx.doi.org/10.1016/j.matdes.2020.109303>.
- [287] Yang C, Wang B, Li D, Tian X. Modelling and characterisation for the responsive performance of CF/PLA and CF/PEEK smart materials fabricated by 4D printing. *Virtual Phys Prototyp* 2017;12(1):69–76. <http://dx.doi.org/10.1080/17452759.2016.1265992>.
- [288] Zhou Y, Yang Y, Jian A, Zhou T, Tao G, Ren L, Zang J, Zhang Z. Co-extrusion 4D printing of shape memory polymers with continuous metallic fibers for selective deformation. *Compos Sci Technol* 2022;227:109603. <http://dx.doi.org/10.1016/j.compscitech.2022.109603>.
- [289] Scaffaro R, Citarrella MC, Catania A, Settanni L. Green composites based on biodegradable polymers and anchovy (*Engraulis encrasicolus*) waste suitable for 3D printing applications. *Compos Sci Technol* 2022;230:109768. <http://dx.doi.org/10.1016/j.compscitech.2022.109768>.
- [290] Oliveux G, Dandy LO, Leeke GA. Current status of recycling of fibre reinforced polymers: Review of technologies, reuse and resulting properties. *Prog Mater Sci* 2015;72:61–99. <http://dx.doi.org/10.1016/j.pmatsci.2015.01.004>.
- [291] Yu Y, Liu H, Qian K, Yang H, McGehee M, Gu J, Luo D, Yao L, Zhang YJ. Material characterization and precise finite element analysis of fiber reinforced thermoplastic composites for 4D printing. *Comput Aided Des* 2020;122:102817. <http://dx.doi.org/10.1016/j.cad.2020.102817>.
- [292] Wang Q, Tian X, Huang L, Li D, Malakhov AV, Polilov AN. Programmable morphing composites with embedded continuous fibers by 4D printing. *Mater Des* 2018;155:404–13. <http://dx.doi.org/10.1016/j.matdes.2018.06.027>.
- [293] Rajeshkumar G, Seshadri SA, Devnani G, Sanjay M, Siengchin S, Maran JP, Al-Dhabi NA, Karuppiah P, Mariadhas VA, Sivarajasekar N, et al. Environment friendly, renewable and sustainable poly lactic acid (PLA) based natural fiber reinforced composites—A comprehensive review. *J Clean Prod* 2021;310:127483. <http://dx.doi.org/10.1016/j.jclepro.2021.127483>.
- [294] Le Duigou A, Correa D, Ueda M, Matsuzaki R, Castro M. A review of 3D and 4D printing of natural fibre biocomposites. *Mater Des* 2020;194:108911. <http://dx.doi.org/10.1016/j.matdes.2020.108911>.

- [295] Hedayati SK, Behravesh AH, Hasannia S, Saed AB, Akhouni B. 3D printed PCL scaffold reinforced with continuous biodegradable fiber yarn: A study on mechanical and cell viability properties. *Polym Test* 2020;83:106347. <http://dx.doi.org/10.1016/j.polymertesting.2020.106347>.
- [296] Hedayati SK, Behravesh AH, Hasannia S, Kordi O, Pourghaumi M, Saed AB, Gashtasbi F. Additive manufacture of PCL/nHA scaffolds reinforced with biodegradable continuous fibers: Mechanical properties, in-vitro degradation profile, and cell study. *Eur Polym J* 2022;162:110876. <http://dx.doi.org/10.1016/j.eurpolymj.2021.110876>.
- [297] Yang T-C. Effect of extrusion temperature on the physico-mechanical properties of unidirectional wood fiber-reinforced polylactic acid composite (WFRPC) components using fused deposition modeling. *Polymers* 2018;10(9):976. <http://dx.doi.org/10.3390/polym10090976>.
- [298] Baley C, Le Duigou A, Bourmaud A, Davies P. Influence of drying on the mechanical behaviour of flax fibres and their unidirectional composites. *Compos Part A Appl Sci Manuf* 2012;43(8):1226–33. <http://dx.doi.org/10.1016/j.compositesa.2012.03.005>.